CDF/PHYS/EXOTICS/10773
June 12, 2012

Rejecting $e \to \gamma_{\text{fake}}$ Candidates With Loose Track Matching

For Use in Searches for New Physics with Photons and $\not\!\!E_T$

Jonathan Asaadi, Adam Aurisano, Daniel Goldin[1],
Jason Nett, and David Toback

Texas A&M University

Abstract

In this note we describe a new method of rejecting $e \to \gamma_{\text{fake}}$ candidates that pass the standard photon identification requirements. This technique is especially useful in searches for new physics with a photon and $\not\!\!E_T$ in the final state, as it helps reject $W \to e\nu \to \gamma_{\text{fake}} + \not\!\!E_T$ events. It is designed to work even for events where the standard offline algorithms do not select the correct primary vertex. In this case, the track isolation variables are not helpful and the Phoenix tracking cannot provide any additional rejection against tracks. Instead of using the standard practice of matching an extrapolated track position to the measured photon position at the calorimeter face, we compare the ϕ_0 and η_{detector} of the closest reconstructed track to the ϕ and η_{detector} of the photon candidate, as measured in the CES. The match also takes into account the resolution of the track reconstruction of hard-brem electrons. We find that this method rejects approximately 73% of electrons that have already passed all the standard isolated photon ID requirements, but is approximately 90% efficient for promptly produced photons that have passed the same requirements.

[1]Corresponding author: goldin@fnal.gov.

Contents

1 Introduction

In this note, we describe a new method of rejecting $e \to \gamma_{\rm fake}$ candidates that pass the standard photon identification requirements. This technique is especially useful in searches for new physics with a photon and $\not\!\!E_T$ in the final state because it helps reject $W \to e\nu \to \gamma_{\rm fake} + \not\!\!E_T$ events. It is designed to work even for events where the standard offline algorithms do not select the correct primary vertex. In this case, the track isolation variables are not helpful [1] and the Phoenix electron rejection algorithm [2] cannot provide any additional rejection against tracks.

This rejection method was constructed for use in a search for new physics in a $\gamma + \not\!\!E_T$ final state. That search is motivated by various models based on Gauge Mediated Supersymmetry Breaking (GMSB). Section 2 presents some examples and the corresponding final states in which they would be sensitive.

While $W \to e\nu \to \gamma_{\rm fake} + \not\!\!E_T$ has been known to be an important background for a long time, we concentrate on one of the most difficult scenarios for the detector: where the primary vertex is not reconstructed. In Section 2.3, we briefly overview the standard electron rejection methods and explain why the standard fake rejection methods, including Phoenix tracking, are not satisfactory for searches like the $\gamma_{\rm delayed} + \not\!\!E_T$ final state. After a description of datasets and photon ID in Section 3, Section 4 shows in more detail how $e \to \gamma_{\rm fake}$ candidates are typically produced. Armed with this understanding, Section 4.1 describes our new method for rejecting electrons that fake photons. In particular, instead of using the standard practice of searching for a track that points to photon candidates at the face of the calorimeter, we compare the ϕ_0 and $\eta_{\rm detector}$ of the closest reconstructed track to the ϕ and $\eta_{\rm detector}$ of the photon candidate, as measured in the CES. The match also accounts for the resolution of the track reconstruction of hard-brem electrons. In Section 5, we present some results and checks of the method. We note for now that the method rejects approximately 73% of electrons that have already passed all the standard isolated photon ID requirements, but is approximately 90% efficient for promptly produced photons that have passed the same requirements. In Appendix A, we describe how the photon timing for $W \to e\nu \to \gamma_{\rm fake} + \not\!\!E_T$ events can be badly mismeasured in such a way as to produce events which fake the $\gamma_{\rm delayed} + \not\!\!E_T$ final state. Finally, in Appendix B, we consider using the charge of the track as an additional handle in rejecting fakes using the product of closest track's charge q and closest track-EM cluster separation $\Delta\phi$ and compare it with our main method.

2 Motivation for $e \to \gamma_{\mathbf{fake}}$ Rejection in Searches for New Physics with $\gamma + \not\!\!E_T$ in the Final State

2.1 Theoretical Motivations: GMSB Production of Events in Final States

There are a number new physics models that produce $\gamma + \not\!\!E_T$ in the final state. Among them are several models of GMSB [3] and unified extra-dimensional (UED) models [4]. In this note, the former is emphasized. One of the special features of GMSB models is that in R-parity conserving scenarios [5], sparticle production always occurs in pairs, which can produce at least one photon and $\not\!\!E_T$ in the final state. This can occur because any sparticle will eventually decay down to a neutralino $\tilde{\chi}_1^0$–the next-to-lightest SUSY particle (NLSP)–with the subsequent decay to a photon and a gravitino ($\tilde{\mathrm{G}}$)–the lightest SUSY particle (LSP) that is stable. The gravitino will leave the detector without interacting, producing $\not\!\!E_T$.

The phenomenology of GMSB at the Tevatron has been studied in detail [6] and can be thought of as having two different types of production mechanisms and two different types of decay mechanisms (summarized in Table 1). When combined, these provide four different final states to be searched for at CDF. We start by discussing the two different production models. In one model, $\tilde{\chi}_1^0$ pairs are produced at the end of decay chains of heavier sparticles. The other model involves direct $\tilde{\chi}_1^0$ pair production, which was proposed in early 2004 [6], but the results have not yet been published by CDF.

The first type, models that produce $\tilde{\chi}_1^0 \to \gamma\tilde{G}$ near the the end of a long decay chain, are the typical models that have been discussed in the literature and searched for at LEP [7], the Tevatron [8], and the LHC [9]. A typical example is encapsulated in what is known as the SPS-8 relationships [10]. In the SPS-8-type scenarios, just above the current Tevatron exclusion limits, the dominant sparticle production mode at the Tevatron is $\tilde{\chi}_1^+ \tilde{\chi}_2^0$ and $\tilde{\chi}_1^+ \tilde{\chi}_1^-$ (Fig. 1). Each will decay to a photon and gravitino, as well as other high energy particles, in the final state. Thus, the final state is two photons, $\not\!\!E_T$ and other large-energy deposits.

The second production mechanism–corresponding to the second row in Tab. 1–is that of direct $\tilde{\chi}_1^0$ pair production, as shown in Fig. 2, which can result in a pair of photons, gravitinos and not much else. We will refer to this mechanism as exclusive production. There are two types of production diagrams to be considered depending on the masses of the lightest Higgs and the $\tilde{\chi}_1^0$ in the model. The first is direct production through an off-shell Z boson. The other is through resonant production of a Higgs boson, an h^0 to be exact. We note that the Higgs production mechanism was not envisioned in Ref. [6], but is well described in generalized GMSB models [11] and can enhance the overall $\tilde{\chi}_1^0$ pair production rate by a factor of about 1,000 if the masses are favorable. Neutralino pair production via an off-shell Z boson will dominate if the Higgs doesn't exist, if the $\tilde{\chi}_1^0$s are too massive to be produced by a Higgs, and/or if

Model	$\tau_{\tilde{\chi}_1^0} \lessapprox 1$ ns	$1 < \tau_{\tilde{\chi}_1^0} < 10$ ns
SPS-8 GMSB Production	$\gamma\gamma + \not\!\!E_T + H_T$	$\gamma_{\text{delayed}} + \not\!\!E_T +$ jets
Higgs-Type Production	Exclusive $\gamma\gamma + \not\!\!E_T$	Exclusive $\gamma_{\text{delayed}} + \not\!\!E_T$

Table 1: We list possible analyses that can be performed to search for GMSB depending on the masses of the sparticles as well as the lifetime of the neutralino in the model.

the other sparticles are too massive to be produced at the Tevatron.

Equally important to the final state phenomenology is the lifetime ($\tau_{\tilde{\chi}_1^0}$) of the lightest $\tilde{\chi}_1^0$. This lifetime splits the final states into two types: *prompt*-type searches, which are most sensitive to a $\tilde{\chi}_1^0$ lifetime of the order of $\lessapprox$ 1 ns, and *delayed*-type searches, which are most sensitive to a $\tilde{\chi}_1^0$ lifetime of the order of 1 to 10 ns. We note that nanosecond $\tilde{\chi}_1^0$ lifetimes are also cosmologically favored and favored for low-scale SUSY breaking [12]. A cartoon version of what a long-lived $\tilde{\chi}_1^0$ would look like inside the detector, shown in Fig. 3, illustrates why delayed searches have the name they do.

Prompt decays produce the $\gamma\gamma + \not\!\!E_T$ final state [8] that has been searched for in the SPS-8 style processes at LEP [7], Tevatron [8] and LHC [9]; exclusive $\gamma\gamma + \not\!\!E_T$, as would be expected from exclusive $\tilde{\chi}_1^0$ pairs, has not yet been published at CDF. Delayed searches have been described in detail in Ref. [6] and [13]. In this case, one of the $\tilde{\chi}_1^0$ is likely to leave the detector before decaying and the other one will decay as in Figure 3, producing a $\gamma_{\text{delayed}} + \not\!\!E_T$ in the final state. Each of the two different production mechanisms thus produce two final states: SPS-8 produces the $\gamma_{\text{delayed}} + \not\!\!E_T +$ jet final state and the exclusive production mechanism produces exclusive $\gamma_{\text{delayed}} + \not\!\!E_T$. The $\gamma_{\text{delayed}} + \not\!\!E_T +$ jet final state has been searched for at the Tevatron [13]. The exclusive $\gamma_{\text{delayed}} + \not\!\!E_T$ search is described in Ref. [14].

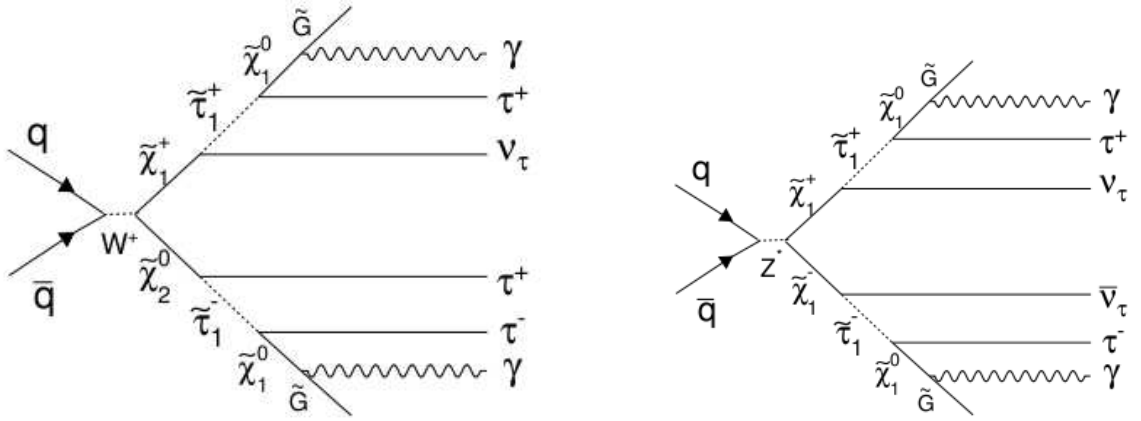

Figure 1: The dominant GMSB sparticle production mechanisms at the Tevatron in SPS-8 versions of GMSB [3] that can produce a photon and $\not\!\!E_T$ in the final state. Just above the current exclusion limits the $\tilde{\chi}_1^{\pm}$ and $\tilde{\chi}_2^0$ are light enough to be produced at the Tevatron, and these processes will dominate. If they are too massive to be produced, then the diagrams in Fig. 2 may dominate.

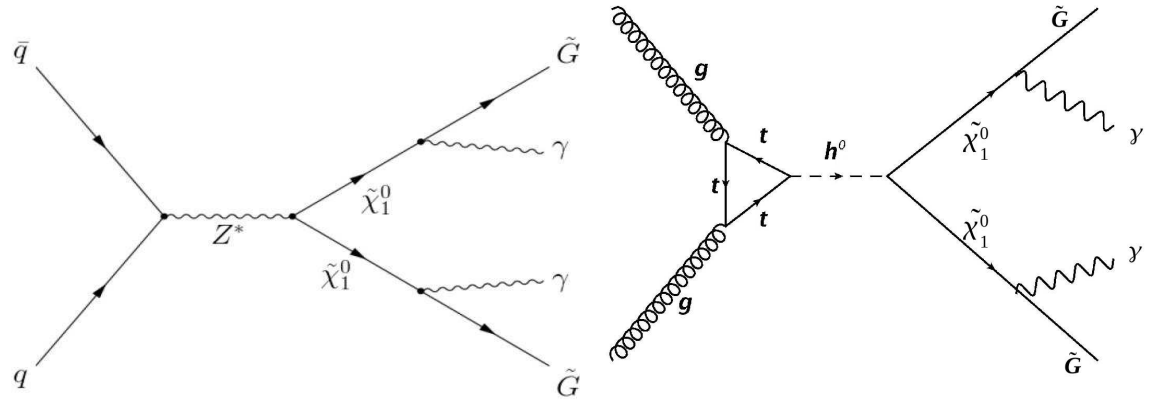

Figure 2: These are the dominant sparticle production mechanisms assuming that all spartices other than the $\tilde{\chi}_1^0$ and the gravitino are too massive to be produced at the Tevatron. On the right, if the Higgs is light enough to be produced on shell and the $\tilde{\chi}_1^0$ is light enough so that this decay can occur (i.e., $M_{\rm Higgs} \gtrsim 2M_{\tilde{\chi}_1^0}$), then this process can dominate. In this case, the ratio of the production cross-sections can be about 1:1000 [11].

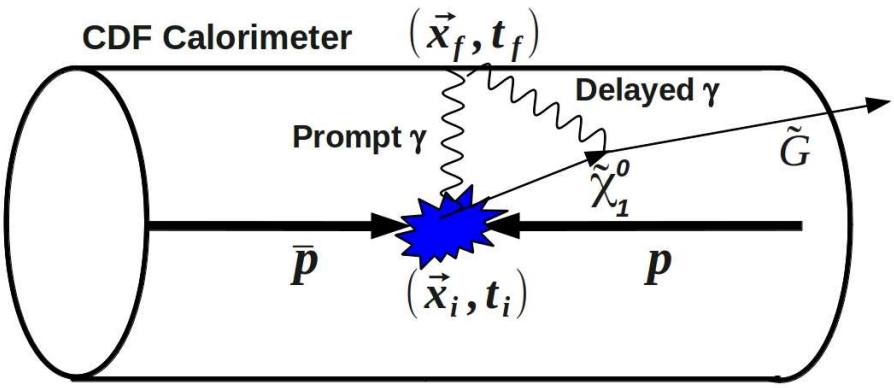

Figure 3: This is an illustration of a long-lived $\tilde{\chi}_1^0$ that decays in flight to a photon and a gravitino inside the detector [15]. In this case, the second $\tilde{\chi}_1^0$ typically escapes the active detector volume. This can produce the $\gamma_{\text{delayed}} + \not{E}_T$ final state.

2.2 Why $W \to e\nu \to \gamma_{\text{fake}} + \not\!\!E_T$ is a Particularly Difficult Background

Now that we have described the four different final states in Table 1, we focus on why electrons from $W \to e\nu \to \gamma_{\text{fake}} + \not\!\!E_T$ require special attention in these searches. This is because (1) they are difficult to reject and (2) electrons that are not typically rejected are especially susceptible to having badly mismeasured timing. This latter issue is discussed in detail in Appendix A and CDF note 9924.

The $W \to e\nu \to \gamma_{\text{fake}} + \not\!\!E_T$ process is a considerable background to any search with a $\gamma + \not\!\!E_T$ in the final state. To really understand why it is particularly difficult and important to reject, we focus on the exclusive $\gamma + \not\!\!E_T$ final state[2]. In the exclusive $\gamma + \not\!\!E_T$ final state, the lack of other final state particles means that there are fewer tracks to produce a vertex. This means that the collision is both less likely to be reconstructed as a vertex and less likely to be selected as the highest ΣP_T vertex, which is used in timing measurements [8] and photon ID [1].

There are a number of reasons why the incorrect selection of the primary vertex is a problem. The main ones are:

- Incorrect selection of the vertex gives an incorrect $\sin\theta$ used in the measurement of $E_T + \not\!\!E_T$.
- Incorrect selection of the vertex results in mismeasured/biased timing (see Appendix A).
- The standard rejection techniques used in photon ID are not as powerful when we most need them. Specifically, the track isolation cut currently requires the tracks considered be within 5 cm of the primary vertex [1].
- As we will see, the Phoenix Tracking algorithms [2], which are premised on the correct selection of the primary vertex, cannot be used effectively to assist us.

In subsections 2.3 and 4.1, we describe the dominant mechanism by which electrons fake photons and illustrate how and where this occurs in the detector. This will more explicitly explain why the various electron rejection techniques won't help when the vertex is not correctly identified. Our new method for rejecting electrons will be discussed in Section 4 after a description of the photon ID and the datasets used in our study (Section 3). This method shows excellent rejection, even when the wrong vertex is selected. We note for now that our method is general enough to be extended to other physics searches with $\gamma + \not\!\!E_T$ in the final state, or any analysis where the correct vertex is not identified. It should also work well against jets that fake photons, although this has not been studied in detail.

[2]It is true that $e \to \gamma_{\text{fake}}$ candidates affect each process differently, but it is most difficult to cope with in the exclusive $\gamma + \not\!\!E_T$ final state for reasons that will be discussed below.

2.3 Why the Standard Electron Rejection Methods Aren't Satisfactory, Especially for Exclusive $\gamma_{\mathbf{delayed}} + \not{E}_T$ Searches

The natural starting point for rejecting electron events that pass photon ID cuts is to alter the existing photon identification cuts to be more stringent in a manner that would help reject $e \to \gamma_{\text{fake}}$ candidates. For example, we could consider loosening the P_T cut of the standard photon track rejection cuts (Table 2) or to use Phoenix tracking [2] to reject $e \to \gamma_{\text{fake}}$ candidates. However, by understanding the typical manner in which electrons fake photons we will readily see why neither approach is suitable in our case, especially when the correct vertex is not correctly identified or used in the offline/ID algorithms.

As we will show in more detail in Section 4, the dominant way that electrons fake photons is when there is a hard-brem in the detector material. A cartoon of the process is shown in Fig. 4. As an electron travels through the detector material, a hard interaction can cause it to lose a large fraction of its energy to a photon. The electron's trajectory is severely affected by the energy and momentum loss; it may either leave a much lower energy deposition in a calorimeter or be swept away completely by the magnetic field of the solenoid. The bulk of the energy of the photon candidate in the calorimeter is thus due to the brem'd photon.

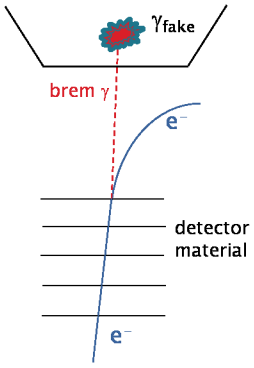

Figure 4: This is an illustration of an electron interacting with the material in the detector and having a hard interaction which gives most of the energy to the photon. The low-P_T electron is highly curved in the magenetic field and will not be matched at the calorimeter face. Note that pre- and post-brem trajectory can sometimes be reconstructed as a single, low P_T track.

We can now see why there are photon candidates remaining after the standard N3D track requirement of the standard photon ID cuts. For electrons where the post-brem electron loses most of its initial momentum and is left with a low enough P_T track, the track is significantly curved away from the final location of the photon candidate in the calorimeter. Since the ϕ position of the low-P_T track at the face of the calorimeter is far from the reconstructed ϕ position of the photon candidate, it can be outside the window to be "matched" to the photon candidate by the offline photon reconstruction

algorithms [1]. For all EM clusters, the standard photon identification matching algorithm searches for the presence of tracks that have an extrapolated calorimeter position near the cluster centroid at the face of the calorimeter. To be considered as "matched," tracks are required to point to the EM cluster within 25 cm in Δx and 38 cm in Δz, where Δx and Δz are measured between the center of the seed EM calorimeter and the extrapolated track position. This corresponds to a distance of one tower in x and two towers in z. We find that a low-P_T brem'd track can end up at least three towers away from the EM cluster. The standard photon track selection cuts require either either 0 or 1 $3D$ tracks pointing at the EM cluster. In the case of only one $3D$ track being found, it is required to have $P_T < 0.025 \cdot E_T$. This is very effective for rejecting electrons in general since the charged track is readily identified and rejected. However, in the case of a hard bream, loosening the P_T cut does not help, since a looser cut would only admit more tracks that have no association with the $e \to \gamma_{\rm fake}$ candidate.

An additional rejection method for electrons and jets that fake photons is track isolation, which rejects any photon candidate if there is greater than 5 GeV of track P_T in a cone of $\Delta R < 0.4$ around the centroid of the photon cluster. This could provide additional rejection against electrons [1]. However, the standard requirement is for the tracks to be matched to within 5 cm of the primary vertex. This does not work when the vertex that produces the electron is not selected for the photon ID algorithms.

A second, more sophisticated, approach of identifying the $e \to \gamma_{\rm fake}$ candidates that pass the standard photon ID requirements is the Phoenix method (for more details on the method see Refs. [17, 18]). The Phoenix algorithm looks for the evidence of SVX hits along the path between the primary vertex z position and the CES cluster position. These hits are then used to guide the SVX pattern recognition software in reconstructing tracks using Kalman filtering techniques [19]. If a track is successfully reconstructed, a photon candidate is rejected as it appears to be from an electron. For the case where the collision that produces the electron also produces the primary vertex, this algorithm rejects about 60% of photon candidates [21], with an efficiency for real photons of 92%. This is very helpful in principle, but in practice it only helps in cases where the right vertex is selected. Events with a correctly reconstructed vertex do not constitute a significant background to searches for $\gamma_{\rm delayed} + \not\!\!E_T$ events, as they rarely fall into our signal timing region (see Appendix A for more details about the timing for wrong vertex events). We also note that the wrong vertex can be selected in 25% of exclusive $W \to e\nu \to \gamma_{\rm fake} + \not\!\!E_T$ events. This occurs because we reject against events with jets produced in association with the W, and this lowers the vertex ΣP_T. The vertex may not be reconstructed and even if it is, additional minimum bias collisions in the event can produce a vertex which is selected as the primary vertex. As shown in Ref. [21] this can happen a significant fraction of the time. The bottom line is that the Phoenix algorithm is often inefficient for our purposes, and since Phoenix tracking only works in the case when the right vertex is reconstructed as the primary vertex, it only helps when we don't need it, and doesn't help when we do.

Since the standard Phoenix tracking is not designed to help in the case where an

event with the wrong vertex is chosen, it is useful to consider a modified Phoenix method to reject these events. Naïvely modifying the Phoenix algorithm to loop over all the vertices as a seed and search for SVX hits along each road to the CES could certainly help for the cases when the right vertex is reconstructed. However, it will not help in the case when it isn't reconstructed. Another possibility is to consider all z collision positions, but this is likely to be very CPU intensive, and in some sense this procedure would replicate the standalone SVX tracking. We will follow up on this option in Section 5.3, after we describe our chosen method.

For all the reasons mentioned above, we have developed a new method that takes advantage of the observation that the majority of the $e \rightarrow \gamma_{\rm fake}$ candidates are due to electrons which interact with detector material and brem. As we will see, the track is often there to be found and can be used to reject the electron. We describe our new method of looping over all tracks in the event and matching them to the photon candidate in Section 4 after discussing the object identification and Data Samples used in our study.

3 Object Identification and Data Samples

In this section, we describe the photon and electron identification requirements (Tables 2 and 3) as well as the requirements used to select and create a number of subsamples of events. We will use these samples to understand how electrons and promptly produced photons interact in the detector in such a way as to be identified as photons and to find the rejection power and efficiency of any algorithm and selection criteria. The cuts on the data samples were made to be as similar as possible to the exclusive $\gamma + \not\!\!E_T$ final state [20], which explains the presence of the track, jet, and cosmics veto cuts. We expect these results to be easily extended to less restrictive cases. Finally, we will check these results with control samples.

We will consider both data and Monte Carlo (MC) samples. We will begin by focusing on the standard MC CDF samples as they allow us to make pure $e \to \gamma_{\rm fake}$ samples. Since it is difficult to create pure samples of fake photons from electrons with real data we will only use them as cross-checks to avoid potential biases. Our first dataset is an MC sample of $W \to e\nu \to \gamma_{\rm fake} + \not\!\!E_T$ events which we use to both understand how electrons fake photons, as well as measure how well we reject $e \to \gamma_{\rm fake}$ events with any new algorithm. In order to measure the retention rate of promptly produced photons, we also select a MC subsample of $Z\gamma \to \nu\nu\gamma \to \gamma + \not\!\!E_T$ and $\gamma_{\rm cosmics} + \not\!\!E_T$ events. We create two samples based on Z's to help cross check our results. A sample of MC events with $Z \to ee \to e\gamma$ as well as a sample of $e\gamma$ events in data allow for a comparison of the two. A further subsample with an invariant mass close to the Z mass is made in an effort to create a modestly pure sample of $e \to \gamma_{\rm fake}$ events in data. Lastly, an MC $W \to e\nu \to e + \not\!\!E_T$ sample is used to compare good electrons to the good tracks in $e \to \gamma_{\rm fake}$ that define $\Delta R_{\rm pull}$.

We next describe each sample:

- The MC sample of $W \to e\nu \to \gamma_{\rm fake} + \not\!\!E_T$ events was selected from the standard $W \to e\nu$ sample (`we0she, we0sge, we0seh, we0sie, we0sej`) that was simulated using the PYTHIA [22] generator to produce W's and their decays to $e\nu$, and CDFSim [23] versions 6.1.4b and 6.1.4f for the different run periods. For more details on how this sample was created see Ref. [24]. Each event was selected by requiring the photon candidate to pass the selection cuts in Table 2, the $\gamma_{\rm fake} + \not\!\!E_T$ event selection cuts in Table 4 and the generator-level cuts in Table 5 to ensure that the photon in these events come from an electron rather than an initial or final state photon. While these requirements are determined and described in the next subsection, we note for now that we require that the calorimeter position of the photon candidate be within a cone of $\Delta R < 0.4$ of the initial electron direction, and that we require the reconstructed photon energy to be between 90% and 110% of the initial electron energy.[3]

[3] The photon energy as a fraction of the initial electron energy being larger than 1 can be accounted for by the initial-state radiation (ISR) found inside the isolation cone $\Delta R < 0.4$, as well as the upward fluctuations in the photon energy measurement.

- The standard MC sample of $Z\gamma \to \nu\nu\gamma \to \gamma + \not\!\!E_T$ events (`zx0s0n`) was simulated using the PYTHIA generator to produce the $Z\gamma$ process, with the subsequent Z decay into $\nu\nu$, with CDFsim 6.1.6f. More sample production details can be found at [24]. All the events are required to pass the cuts in Table 4.

- In an attempt to create a modestly pure sample of $e \to \gamma_{\rm fake}$ events in $Z \to ee \to e\gamma$ data, we select a set of events with a photon and electron candidate passing all the tight ID (see Table 6). The events are selected from the `bhelbh/bj/bi/bk/bm` streams. The photon candidate is required to pass the cuts in Table 2, and the electron candidate is required to pass the cuts in Table 3. To create a modestly pure sample of $e \to \gamma_{\rm fake}$ events we create a further subsample of events which are consistent with having come from a $Z \to ee \to e\gamma_{\rm fake}$ by virtue of an invariant mass requirement as shown in Table 6.

- The MC sample of $Z \to ee \to e\gamma$ events was derived from the standard MC $Z \to ee$ sample (`ze0scd, ze0sdd, ze0sed, ze0see, ze0seh, ze0sei, ze0sej, ze1s6d, ze1sad`). It was simulated using the PYTHIA [22] generator to produce $Z \to ee$ events, and CDFSim [23] versions 6.1.4b and 6.1.4f for the different run periods. Each $e\gamma$ event was selected by requiring the photon candidate to pass the cuts in Table 2, the offline event cuts in Table 6. A further subset of these events are selected using the requirements in Table 5 to create an MC sample of $Z \to ee \to e\gamma_{\rm fake}$.

- The data sample of $\gamma_{\rm cosmic} + \not\!\!E_T$ events are selected from the `bhel*` stream with the requirements described in Table 4. In order to separate the cosmics from Standard Model-type collisions, we also require that the raw[4] EMTiming time be between 20 and 80 ns and that the candidate not come from a beam halo candidate. The full set of requirements is summarized in Table 7.

- The standard MC sample of $W \to e\nu \to e + \not\!\!E_T$ events was simulated in the same way as above, but each event is required to pass the cuts in Table 8. This sample is used in Fig. 15 to compare the tracks in $e \to \gamma_{\rm fake}$ events to electrons in $W \to e\nu \to e + \not\!\!E_T$.

With these datasets and cuts, we next turn to our rejection techniques and the measurement of our efficiency and rejection power.

[4] We note that no use is made of the vertex in the calculation of the timing.

Quantity	**Selection Cut**
EM cluster E_T	1 cluster with $E_T > 30$ GeV
Fiducial	$\lvert X_{\rm CES}\rvert < 21$ cm and $9 < \lvert Z_{\rm CES}\rvert < 230$ cm
Hadronic fraction	$E_{\rm HAD}/E_{\rm EM} < 0.125$
Energy isolation	$E^{\rm iso}_{\rm cone\ 0.4} < 2.0 + 0.02 \cdot (E_T - 20.)$
1st CES cluster energy ($E_{\rm CES}$ cut)	$E^{\rm 1st}_{\rm strip} + E^{\rm 1st}_{\rm wire} > 10$ GeV
2nd CES cluster energy	The bigger quantity of the CES 2nd cluster strip or wire energies required to be smaller than one of the two corresponding sliding cuts: (1) if photon $E_T < 18$ GeV: $E^{\rm 2nd}_{\rm CES} < 0.14 E_T$ (2) if photon $E_T > 18$ GeV: $E^{\rm 2nd}_{\rm CES} < 2.4 + 0.01 \cdot E_T$
PMT spike rejection	$A_{\rm PMT} = \frac{\lvert E_{\rm PMT1} - E_{\rm PMT2}\rvert}{E_{\rm PMT1} + E_{\rm PMT2}} < 0.6$
Track Multiplicity	Number of N3D tracks either 0 or 1
Track P_T	If $N3D = 1 \rightarrow P_T < 1.0 + 0.005 \cdot E_T$
Track isolation	$\Sigma P_T < 5$ GeV
Cosmics Rejection	Reject events with any of the following: (1)$\Delta\phi(\gamma$, closest stub$) < 30$ degrees; (2)HadE $> -0.3 + 0.008 \cdot E^0_{\rm T}$; (3)CES E/E > 0.2 [28]

Table 2: The good photon selection cuts. Note that these are standard photon ID cuts for high E_T photons [1], with the following exceptions described in Ref. [18]: the standard $\chi^2_{\rm CES}$ cut is removed, and the PMT asymmetry cut to reject PMT spikes, and two new cuts on HadE and CES E/E to reject cosmics.

Quantity	**Selection Cut**
EM cluster E_T	1 cluster with $E_T > 45$ GeV
Fiducial	$\lvert X_{\rm CES}\rvert < 21$ cm and $9 < \lvert Z_{\rm CES}\rvert < 230$ cm
Hadronic fraction	$E_{\rm HAD}/E_{\rm EM} < 0.055 + 0.00045 \cdot E_{\rm EM}$
Energy isolation	$E^{\rm iso}_{\rm cone\ 0.4} < 0.1 \cdot E^{\rm EM}_T$
2nd CES cluster energy	$E^{\rm 2nd}_{\rm CES} < 2.4 + 0.01 \cdot E_T$
$L_{\rm shr}$	< 0.2
Track $P_T$and E/p	Track P_T> 50 GeV, if P_T< 50 GeV, require $E/p < 2$

Table 3: Good electron selection requirements. Taken from [25]. Note that these are standard electron ID cuts, with the exception of $\chi^2_{\rm CES}$ cut, which has been removed.

Quantity	**Selection Cut**
Trigger (applied to data only)	`W_NOTRACK or SUPER_PHOTON70 or PHOTON25_ISO or ULTRA_PHOTON50`
Good photon passing the ID cuts in Table 2	1 cluster with $E_T >$ 30 GeV
$\not\!\!E_T$ $(z = 0)$	$>$ 30 GeV
Veto on any jet not identified as the leading photon	$E_T >$ 15 GeV
Track veto	$P_T >$ 10 GeV NCotAxSeg(5)$\geq$ 2 Total number COT hits greater than 0.6 times the hits last COT layer
Vertex selection [26]	Require at least one spacetime [27] vertex with: $\Sigma P_T >$ 5.0 GeV $\lvert Z_0 \rvert <$ 60.0 cm $N_{\rm Tracks} \geq 3$

Table 4: The set of requirements to create the various $\gamma + \not\!\!E_T$ samples. Note that the track and jet vetos were imposed to reproduce the exclusive $\gamma + \not\!\!E_T$ final state search [20], since our method will be used there.

Quantity	**Selection Cut**
Require photons to pass the cuts in Table 2	
Photon candidate/generator-level electron match	$\Delta R <$ 0.4
Reconstructed photon energy requirement	$90\% < E^{\gamma}_{\rm rec}/E^{e}_{\rm gen} < 110\%$

Table 5: The set of requirements to ensure that the $e \rightarrow \gamma_{\rm fake}$ candidates under consideration in MC are from electrons. These cuts will be used to make the MC $W \rightarrow e\nu \rightarrow \gamma_{\rm fake} + \not\!\!E_T$ and $Z \rightarrow ee \rightarrow e\gamma_{\rm fake}$ samples. For more details, see Figs. 5,6, and 7.

Quantity	**Selection Cut**
Trigger (applied to data only)	`bhelbh/bi/bj/bk/bm` stream selection
Good electron selection	Require 1 electron from Table 3
Good photon selection	Require 1 photon from Table 2
Z mass	Require Z mass constraint: $81 < \|M_{e\gamma}\| < 101$ GeV

Table 6: The $e\gamma$ sample selection requirements. This sample is used to try to select $Z \to ee \to e\gamma_{\rm fake}$ events for cross-checking of our $e \to \gamma_{\rm fake}$ rejection method. Both the electron and photon are cut at 30 GeV. We note that only some of the figures are made with the Z mass requirement. In addition, we will sometimes make the $e \to \gamma_{\rm fake}$ requirements in Table 5.

Quantity	**Selection Cut**
An exclusive $\gamma + \not\!\!E_T$ event passing all the requirements in Table 4, except for the vertex selection and cosmics rejection.	
Raw EMTiming [17]	[20, 80] ns
Beam halo candidate rejection requirements [29]	
Number of CEM Towers	$N_{\rm CEM} > 9$
Number of PHA Towers	$N_{\rm PHA} > 2$

Table 7: The $\gamma_{\rm cosmics} + \not\!\!E_T$ data selection requirements.

Quantity	**Selection Cut**
Electron	Good electron passing the cuts in Table 3
$\not\!\!E_T(z = 0)$	> 45 GeV

Table 8: The $e + \not\!\!E_T$ event selection requirements. No trigger requirement is made since we do not use $e + \not\!\!E_T$ events from data.

4 Rejecting $e \to \gamma_{\mathbf{fake}}$ Candidates

In the sections that follow, we illustrate the physics of $e \to \gamma_{\text{fake}}$ candidates in more detail. This will illuminate why the standard methods of rejecting electron fakes are ill-suited for the case when the wrong vertex is selected and in searches for new physics in the exclusive $\gamma_{\text{delayed}} + \not\!\!E_T$ final state. We will then describe our method, its rejection power and efficiency, and give more details about its effect on the $W \to e\nu \to \gamma_{\text{fake}} + \not\!\!E_T$ sample.

4.1 The Nature of $e \to \gamma_{\mathbf{fake}}$ Candidates and an Overview of Our Rejection Method

In order to illustrate the nature of $e \to \gamma_{\text{fake}}$ candidates, we use an MC $W \to e\nu$ sample with a photon passing all the requirements in Table 2 and the $\gamma + \not\!\!E_T$ requirements of Table 4. We start by creating a set of requirements to separate out MC events where the photon candidate is from an initial or state photon from those where it comes from an electron. Since an electron resulting from the $W \to e\nu$ decay is highly boosted, in the event of a bremsstrahlung interaction with the detector material the outgoing photon and electron have a very small angular separation. Thus, we expect that the reconstructed energy of the photon to be mostly that of the original electron, and that the original electron and the outgoing photon will largely be in the same direction. The ratio of energies vs. the ΔR between the two (reconstructed photon and generator level electron), for all events with a reconstructed photon in our sample, is shown in Figure 5. Most of the events have the reconstructed tight photon around the same energy as the initial electron ($E^{\gamma}_{\text{rec}}/E^{e}_{\text{gen}} \approx 1$) and cluster at $\Delta R \lessapprox 0.4$. These observations allow us to impose the set of cuts shown in Table 5; from here on out we will refer to candidates that pass the requirements in Table 5 as being $e \to \gamma_{\text{fake}}$. As described in the caption in Figure 5, the various ΔR and energy distributions between the other combinations of objects in the event show that the rest of the photons are due to ISR and FSR.

With the subsample of events passing the cuts in Table 5, we can study the processes by which electrons fake photons. As we will see, the overwhelming majority of events are due to an electron that has a hard brem in the detector. We follow the generator electron as it traverses the material in CDFSim [23]and observe that most of the fakes are due to hard brem interactions. There will be many interactions with the material, but if we select the location of the largest transfer of energy to a single photon we can get a sense of what is going on. In Figure 6, we plot the fraction of the energy lost to the photon when we consider the single most energetic brem-interaction. We find that 93% of the time the electron gives more than 50% of its energy to a single photon. The remaining 7% are most likely tracking failures. Thus, we focus on hard-brem interactions as the primary cause of $e \to \gamma_{\text{fake}}$ candidates.

A simple requirement of fraction of the energy lost to be greater than 50% does a fine job of selecting hard-brem events and allows us to map out the locations of

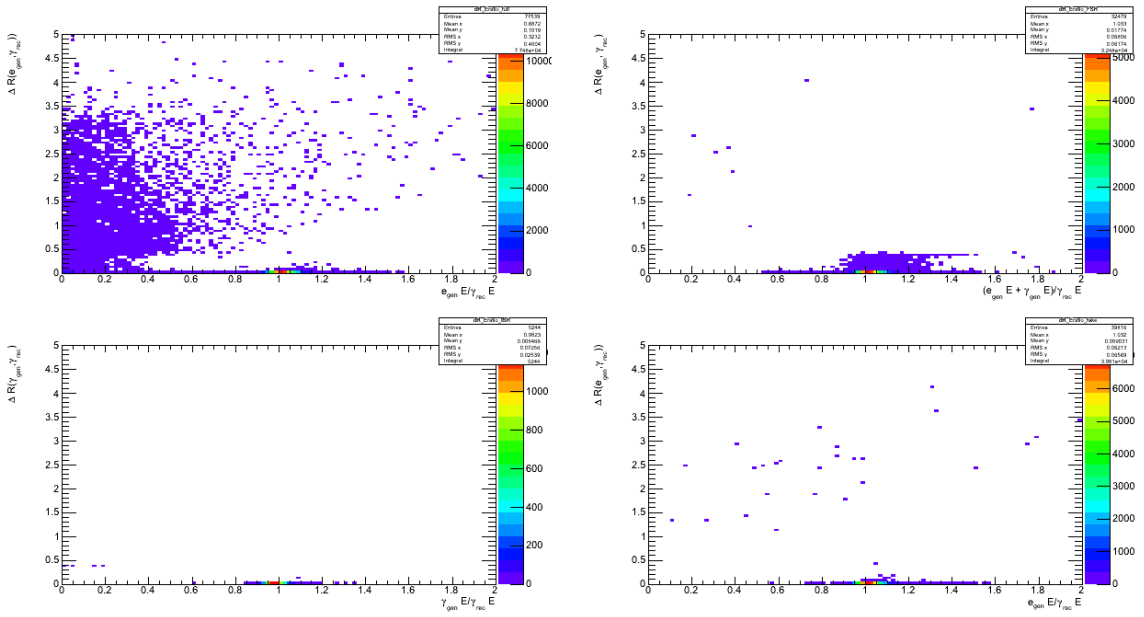

Figure 5: These plots show the relationship between identified photons and generator electrons in $W \to e\nu \to \gamma \not{E}_T$ events. The top left plot shows $\Delta R(\gamma_{\rm rec}, e_{\rm gen})$ vs. the ratio of the generator electron energy to the reconstructed photon energy, which includes the fakes as well as FSR and ISR. The fakes can be seen as having low ΔR and an energy ratio near one. Top right: the ratio of $E^e_{\rm gen} + E^\gamma_{\rm gen}$ over the reconstructed photon energy with ΔR between the $e_{\rm gen}$ and $\gamma_{\rm rec}$ is less than 0.4. This plot shows that many of the events with reconstructed photons are from FSR. Bottom left: There are many events where the photon is at a large angle from the electron. This is the case where the photon is from ISR. To show this, we plot the events where ΔR between the $e_{\rm gen}$ and $\gamma_{\rm rec}$ is less than 0.4 that *are not* in the FSR sample, showing mostly ISR. Bottom right: After removing events that are neither FSR, nor ISR, we see that the remaining events are where the electron faked the photon. As we will see in Figure 6, these are overwhelmingly hard brem events.

the hard bremsstralung interaction inside the detector. This is shown on the left in Fig. 7. In the right-hand-side of Fig. 7, we show the distribution of the integrated fraction (of the total number of brem events) as a function of polar radius at which the bremsstrahlung process occurred is shown in the right figure. Both plots show that most of the brem events occur in the silicon layers and port cards. This is expected as this is where most of the detector material resides in the tracking chamber.

Since we can reasonably expect to find the electron track in the tracking chambers in the event of hard brem, we use this idea as the basis for a new method of electron rejection where we search for the presence of a track that could be associated with an electron. Since a track associated with an electron before bremsstrahlung is close to the final location of the resulting EM cluster, we focus on the separation between the

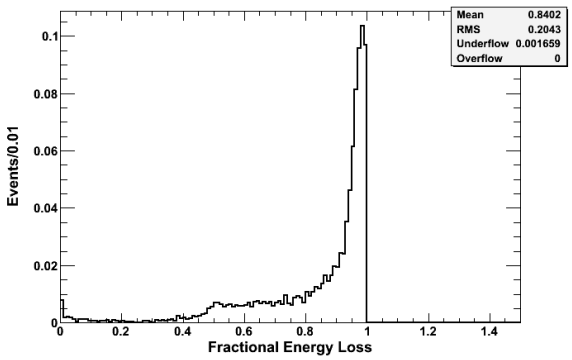

Figure 6: Fraction of total energy lost by the initial electron to the outgoing photon in a single interaction for the sample of events passing the requirements in Table 5. We note that over 93% of the electrons that fake photons have over 50% of their energy bremmed in a single interaction with the detector material.

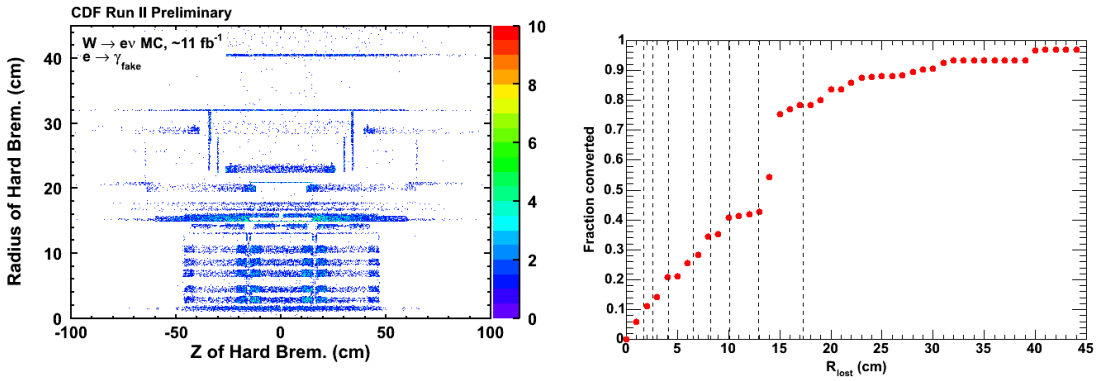

Figure 7: Left: A 2-D plot showing the points inside the detector where electrons suffered a hard brem, where the outgoing photon takes 50%, or more, of the electron's initial energy. Right: An integral plot of the fraction of the events where electron in the MC $W \to e\nu \to \gamma_{\text{fake}} + \not\!\!E_T$ process bremmed as a result of the interaction with the detector material as a function of radius. Most of the brem events are seen to occur in the silicon detector and the port cards (dashed lines).

track closest to the identified photon and the photon itself. This is different from the standard track-matching procedure, which looks for this separation between the photon and the extrapolated track position at the calorimeter face. To be more explicit, we use the ϕ at the beamline (ϕ_0) and η_{det} of the track, then compare to the analogous coordinates for the photon using the CES. This type of matching allows us to introduce an appropriate matching cut.

In what follows, we will see that we can improve our rejection of electrons-faking-photons while retaining high efficiency for real, prompt photons by accounting for the detector response in $\Delta\eta$ and $\Delta\phi$ to hard-brem events. We can also quantify these

quantities for any choice of selection requirements using our sample, and choose the combination that is best for our analysis.

As a way of balancing the rejection power for eliminating the fakes *vs.* the efficiency of retaining promptly produced photons, we start by considering the photon candidate's closest track separation in η-ϕ space for both our MC $Z\gamma \to \nu\nu\gamma \to \gamma + \not\!\!E_T$ sample and our fake-photon sample MC $W \to e\nu \to \gamma_{\text{fake}} + \not\!\!E_T$ events. We compare the distributions of both samples and define the "zeroth-order" selection variables. In the following subsection, this selection will be refined to account for the detector response in $\Delta\eta$ and $\Delta\phi$. The final cut will be defined in terms of the new variable, which we will denote ΔR_{pull}. We will compare the results to data in Section 5.

4.2 Crude Rejection Using Photon-Track Matching in $\eta - \phi$ Space

Our first "zeroth-order" approach identifies fake candidates by looking for a track and considering its η_{detector} and ϕ_0 variables (i.e., its ϕ at closest approach to the beam line). These variables are then compared to the location of the photon candidate in the calorimeter as measured in the CES.

We begin by defining four variables: two pertaining to tracks and two pertaining to the photon candidate. The track variables we use are:

- $\phi_{\text{track}} \equiv \phi_0$, corresponding to initial polar angle of the track (`fPhi0` in the `TStnTrack` class [30] [31]).
- η_{track}, corresponding to the track's pseudorapidity relative to the detector origin ($z = 0$), also frequently referred to at CDF as η_{detector} (transformed from the event variable `fEta` in the `TStnTrack` class using the `TStntuple::DetEtaFromEta` method).

The two photon variables are:

- ϕ_{photon}, corresponding to the ϕ coordinate of the photon cluster as measured by the CES (`fPhi` in the `TStnPhoton` class [32])
- η_{photon}, corresponding to the η coordinate of the photon cluster as measured by the CES, relative to the detector origin ($z = 0$), also frequently referred to at CDF as η_{detector} (`fDteta` in the `TStnPhoton` class).

We note that in this study we use only the coordinates relative to $z = 0$ of the detector and not to the primary vertex, because the true collision point may either be misidentified or not reconstructed.

With these definitions, the angular separation between the tracks and photons in the η-ϕ detector coordinate space becomes:

$$\Delta\eta \equiv \eta_{\text{photon}} - \eta_{\text{track}} \tag{1}$$

and

$$\Delta\phi \equiv \phi_{\text{photon}} - \phi_{\text{track}}. \tag{2}$$

We will make use of the ΔR variable defined in a standard way using quantities found in Eq. 1 and 2:

$$\Delta R = \sqrt{(\Delta\eta)^2 + (\Delta\phi)^2} \tag{3}$$

Our "zeroth-order" approach of identifying fake candidates is straightforward: loop over all good tracks (defined as tracks with number of axial and stereo COT layers with five or more hits, `NAxSeg(5)` ≥ 2 and `NStSeg(5)` ≥ 2) in the event to find the closest one in ΔR. This procedure is run on the events in the MC $W \to e\nu \to \gamma_{\text{fake}} + \not\!\!E_T$ sample and the MC $Z\gamma \to \nu\nu\gamma \to \gamma + \not\!\!E_T$ sample. We plot the results in Figs. 8 and 9, as well as in ΔR in Fig. 9, left. This approach provides a reasonable separation power between the photons and the fake candidates, if one chooses to define a cut on ΔR or a set of cuts on $\Delta\eta$ and $\Delta\phi$ separately.

On the other hand, for the $\Delta\phi$ distribution in Fig. 8, and even more clearly so in Fig. 9, right, the detector response in $\Delta\phi$ is significantly broader than in $\Delta\eta$. This is not surprising, given the presence of the magnetic field acting in the r-ϕ plane. This impacts the curvature of the electron differently before and after the hard brem. The tracking algorithm assumption of a single trajectory for this unusual case can cause a significant mismeasurement of the original P_T and/or ϕ_0. With this in mind, we set out to "equalize" the distributions in $\Delta\eta$ and $\Delta\phi$, accounting for the detector response, thus improving the separation between the fakes and the real photons.

Before proceeding with the description of our final method, we note that we tried accounting for the charge-curvature relation for charged particles in a magnetic field. Since the curvature of the electron track is correlated with the charge, the sign of the product $q\Delta\phi$, where q is the charge associated with the track and $\Delta\phi$ is defined in Eq. 2, should always be positive for all the events. We found that for the case of electrons a cut on the sign of $q\Delta\phi$ did not improve the rejection and only slightly helped the efficiency. This could be employed for high occupancy events where there are typically more than 100 tracks in the event. For more details see Appendix B where we also considered $q\Delta\phi \times P_T$.

4.3 Accounting For Tracking Response

As discussed in the previous section, our "zeroth-order" approach to separating $e \to \gamma_{\text{fake}}$ from real photons is powerful, but limited in that it doesn't account for the different detector responses. The detector response may be found from the Gaussian fits in $\Delta\eta$ and $\Delta\phi$ to the bulk of the fake candidate distributions found in Fig. 8. The large tails are determined to be from uncorrelated tracks. As seen from the results in Fig. 8, the response in $\Delta\eta$ and $\Delta\phi$ is $\sigma_\eta = 6.3 \cdot 10^{-3}$ and $\sigma_\phi = 8.1 \cdot 10^{-2}$, respectively. We can now define the new "pull" $\Delta\eta$ and $\Delta\phi$ variables which account for the detector response.

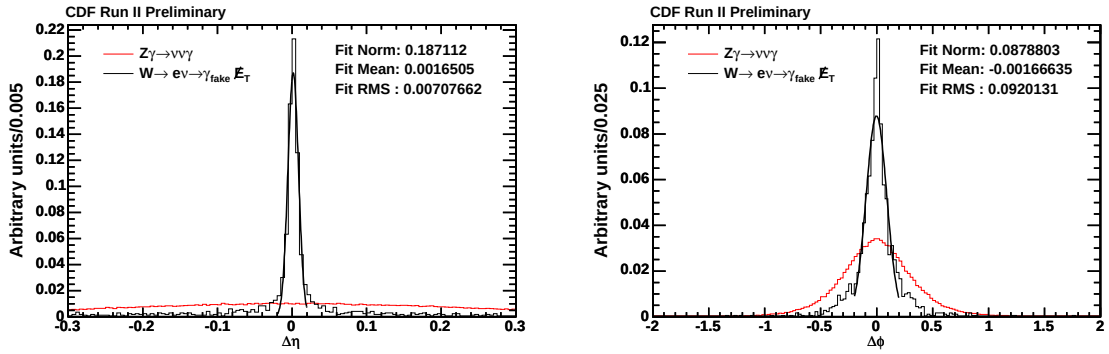

Figure 8: The closest track-photon distributions in $\Delta\eta$ and $\Delta\phi$ for the MC $Z\gamma \to \nu\nu\gamma \to \gamma + \not{E}_T$ sample (red) and the MC $W \to e\nu \to \gamma_{\text{fake}} + \not{E}_T$ sample of fakes (black). The $\Delta\phi$ distribution for fake candidates is markedly worse than $\Delta\eta$ due to the presence of the magnetic field. (Note the different x-axis ranges in the two plots.)

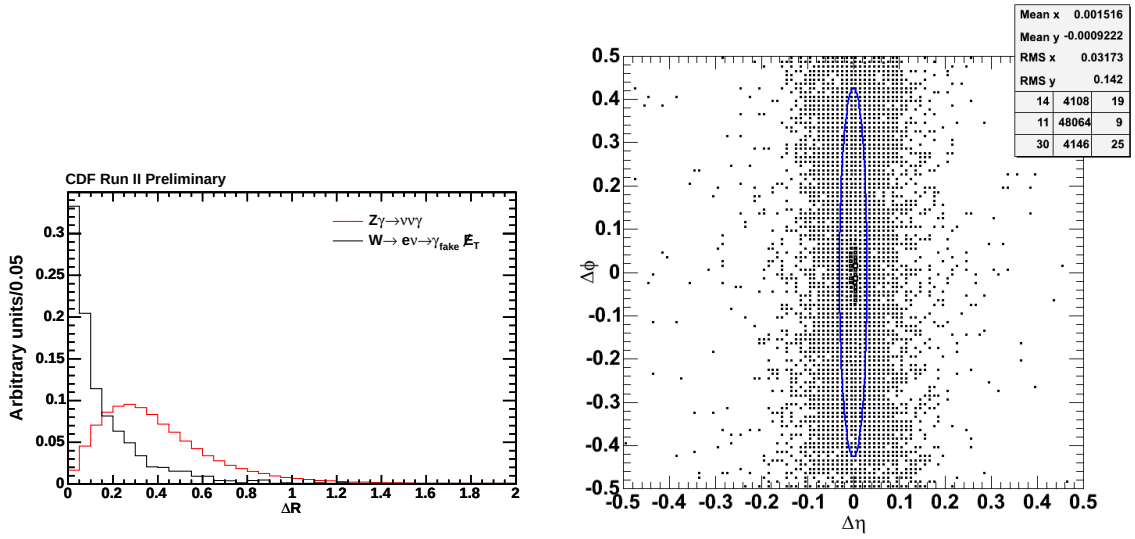

Figure 9: Left: The closest track-photon distributions in ΔR for the MC $Z\gamma \to \nu\nu\gamma \to \gamma + \not{E}_T$ sample (red) and the MC $W \to e\nu \to \gamma_{\text{fake}} + \not{E}_T$ sample (black) of fakes. Right: The photon-closest track $\Delta\phi$ vs. $\Delta\eta$ for the MC $Z\gamma \to \nu\nu\gamma \to \gamma + \not{E}_T$ sample. The oval indicates the $\Delta R_{\text{pull}} > 5$ cut discussed in Section 4.3.

With the definitions of Eq. 1 and 2 we take:

$$\Delta\eta_{\text{pull}} \equiv \frac{\Delta\eta}{\sigma_\eta} \tag{4}$$

$$\Delta\phi_{\text{pull}} \equiv \frac{\Delta\phi}{\sigma_\phi} \tag{5}$$

The distributions for the two variables are plotted in Fig. 10. Their shape is essentially the same as those in Fig. 8, but with the widths "stretched" by dividing by σ_η and σ_ϕ, respectively.

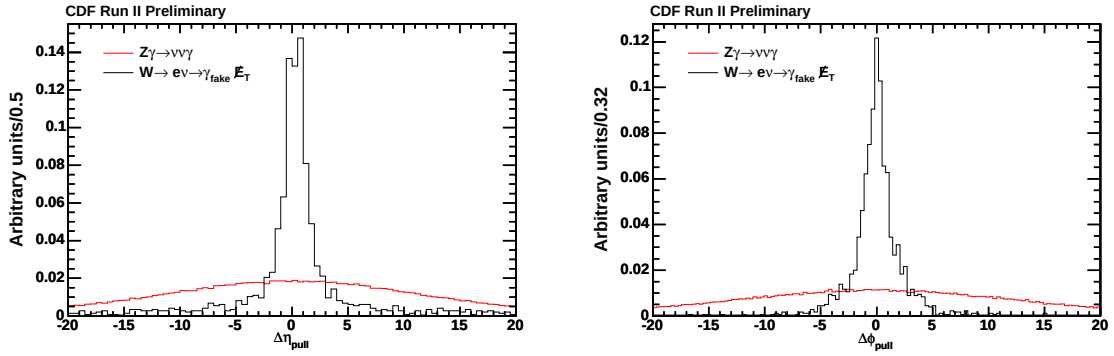

Figure 10: The closest track-photon distributions in $\Delta\eta_{\text{pull}}$ and $\Delta\phi_{\text{pull}}$ for the control sample (red) and the sample of γ_{fakes} (black).

In analogy with Eq. 3 and using Eq. 4 and 5, we define another variable, ΔR_{pull}, as:

$$\Delta R_{\text{pull}} = \sqrt{(\Delta\eta_{\text{pull}})^2 + (\Delta\phi_{\text{pull}})^2}. \tag{6}$$

We again loop over all good tracks, this time selecting the track with the smallest ΔR_{pull}. The ΔR_{pull} distribution (to be compared to the "standard" ΔR in Fig. 9) is shown in Fig. 11, noting that applying the "pull" factors has the effect of equalizing the detector response in $\Delta\eta$ and $\Delta\phi$. As seen in the figure, ΔR_{pull} distributions allow for a better separation between the MC $Z\gamma \to \nu\nu\gamma \to \gamma \not\!\!E_T$ sample and the sample of fakes.

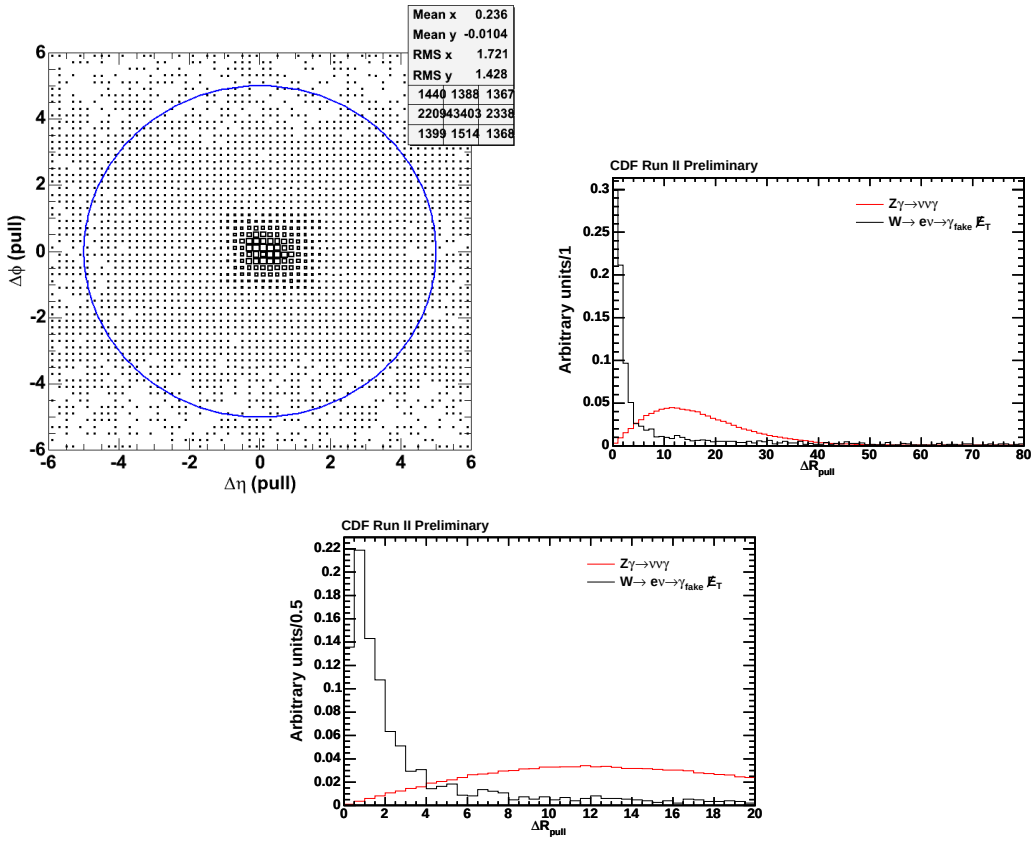

Figure 11: Left: Dividing $\Delta\eta$ and $\Delta\phi$ distributions by their respective pulls yields a more symmetric distribution in $\Delta\eta_{\text{pull}}$ and $\Delta\phi_{\text{pull}}$ than between "standard" $\Delta\eta$ and $\Delta\phi$ (cf. Fig. 9). top right and bottom (zoomed-in version): The closest track-photon distributions in ΔR_{pull} for the control sample and the sample of fakes. Making a cut on "pull" ΔR provides a better MC $Z\gamma \to \nu\nu\gamma \to \gamma + \not{E}_T$ efficiency and $e \to \gamma_{\text{fake}}$ rejection power than simply cutting on ΔR . Note that both samples are set to the same normalization.

4.4 Results: Efficiency and Rejection

We next consider the efficiency and rejection power as a function of a $\Delta R_{\rm pull}$ cut value. We define the efficiency to be the fraction of events *remaining* in the MC $Z\gamma \to \nu\nu\gamma \to \gamma + \not\!\!E_T$ sample after the $\Delta R_{\rm pull}$ cut:

$$\epsilon_{\rm eff} = \frac{N_c(\Delta R_{\rm pull} > \Delta R_{\rm pull}^{\rm cut})}{N_c}, \tag{7}$$

where $N_c(\Delta R_{\rm pull} > \Delta R_{\rm pull}^{\rm cut})$ is the number of events in the MC $Z\gamma \to \nu\nu\gamma \to \gamma + \not\!\!E_T$ sample passing the $\Delta R_{\rm pull}^{\rm cut}$ cut and N_c is the total number of events in this sample. Analogously, we define the rejection as the fraction of events *rejected* by the $\Delta R_{\rm pull}$ from the $e \to \gamma_{\rm fake}$ samples as:

$$\epsilon_{\rm rej} = \frac{N_f(\Delta R_{\rm pull} < \Delta R_{\rm pull}^{\rm cut})}{N_f}, \tag{8}$$

where $N_f(\Delta R_{\rm pull} < \Delta R_{\rm pull}^{\rm cut})$ is the number of events in the MC $W \to e\nu \to \gamma_{\rm fake} + \not\!\!E_T$ sample rejected by the $\Delta R_{\rm pull} < \Delta R_{\rm pull}^{\rm cut}$ cut and N_f is the total number of events in this sample.

With these two definitions, we step through a sequence of $\Delta R_{\rm pull}^{\rm cut}$ values, recording $\epsilon_{\rm eff}$ and $\epsilon_{\rm rej}$ for each. The results are shown in Fig. 12, left. The rejection vs. efficiency is shown on the right hand side. To balance the efficiency and rejection, we set the value of $\Delta R_{\rm pull}^{\rm cut} > 5$, as it is a reasonable approximate position of the inflection point. With this value we find that we accept roughly 95% of MC $Z\gamma \to \nu\nu\gamma \to \gamma + \not\!\!E_T$ sample events, while rejecting approximately 73% of fakes. This rejection is about what is expected from Phoenix rejection [2] in the assumption that the right vertex has been selected (using the second electron leg). The efficiency for the Phoenix method is 60%, while the efficiency of our $\Delta R_{\rm pull}$ cut is 95%.

4.5 Discussion

We next look in more detail at the events rejected by our cut, as well as those that remain in our sample. Using our MC $W \to e\nu \to \gamma_{\rm fake} + \not\!\!E_T$ sample, we can verify the earlier claim that the electron conversions in hard-brem events occurred mostly before the entrance to the COT. This is the case, as illustrated in Fig. 13. The square markers show the integral fraction of events rejected by the $\Delta R_{\rm pull}> 5$ cut, while the circle markers indicate the integral fraction of the *total* number of events in the sample. The bottom curve flattens out at roughly 73%, which corresponds to the rejection rate of the $\Delta R_{\rm pull}> 5$ cut. A kink at around 15 cm corresponds to the location of the port cards where a big fraction of hard-brem events occurred.

In Fig. 14 we observe that the rejection rate shows no dependence on photon E_T for two MC samples with $e \to \gamma_{\rm fake}$, one from $W \to e\nu \to \gamma_{\rm fake} + \not\!\!E_T$ and the other from $Z \to ee \to e\gamma_{\rm fake}$ (the latter to be discussed in more detail in Section 5.1). The P_T distribution of the good tracks for the sample of $W \to e\nu \to \gamma_{\rm fake} + \not\!\!E_T$ events

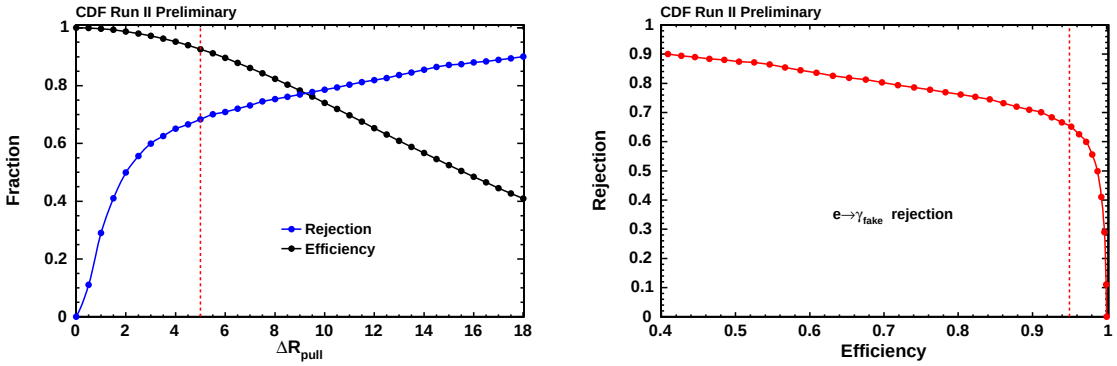

Figure 12: The efficiency and rejection power of our cut as a function of $\Delta R^{\rm cut}_{\rm pull}$. Note that a cut at $\Delta R_{\rm pull}$= 5 (red dashed line) results in approximately 95% efficiency of MC $Z\gamma \to \nu\nu\gamma \to \gamma + \not\!\!E_T$ and 73% rejection of $e \to \gamma_{\rm fake}$ candidates.

that are rejected by the $\Delta R_{\rm pull}$> 5 cut is shown in the left Fig. 15. In the right and bottom figures, we show the number of axial and stereo COT segments associated with these tracks along with a comparison of the axial and stereo hit information with those for a good electron (sample passing the cuts in Table 8). It is clear that these are well-measured tracks, consistent with our hypothesis that they are low P_T post-brem electrons.

In Fig. 16, we show the timing distributions for the sample of $W \to e\nu \to \gamma_{\rm fake} + \not\!\!E_T$ events before and after the $\Delta R_{\rm pull}$> 5 cut. Of particular interest is the shape and normalization of the "wrong vertex" events. A double Gaussian fit shows that the mean stays roughly the same, but that the normalization goes down significantly. The effect of the cut is quantified in Table 9. Our signal region (denoted by "SR") spans the [2,7] ns interval, while the "wrong-vertex sideband" (NVS) region is [-7,-2] ns. We find that while the mean of the fit stayed relatively constant, the total number of events in the signal region has decreased by 67%. Meanwhile, the number of events in the no-vertex sideband region decreased by a greater fraction, at 72%. This is also evident in the $\frac{N_{\rm SR}}{N_{\rm NVS}}$ ratio, which was 1.50 ± 0.12 before and 1.88 ± 0.38 after the cut, both consistent within errors.

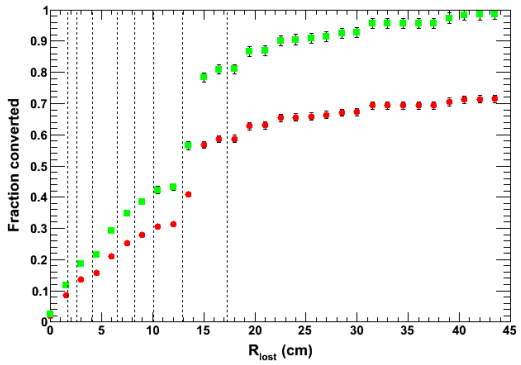

Figure 13: An integral plot of the fraction of the events where the electron in the MC $W \to e\nu \to \gamma_{\text{fake}} + \not\!\!E_T$ sample bremmed as a result of the interaction with the detector material as a function of radius. The filled green squares show the integral fraction of *rejected* events, while the filled red circles the integral fraction of the *total* number of events in the sample. Most of the brem events are seen to occur in the silicon detector and the port cards.

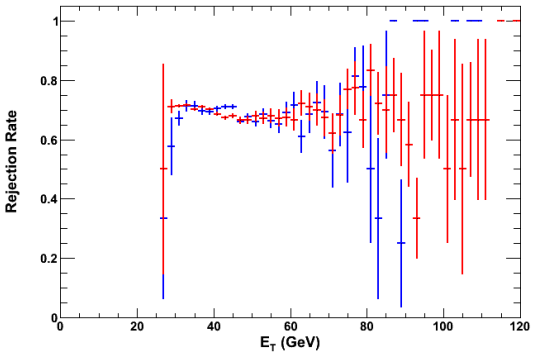

Figure 14: Rejection rate as a function of E_T for MC $Z \to ee \to e\gamma_{\text{fake}}$(blue) and MC $W \to e\nu \to \gamma_{\text{fake}} + \not\!\!E_T$ (red) events. The ratio is flat across the E_T spectrum.

	Signal region (SR) [2,7] ns	**Wrong-Vertex Sideband (NVS) [-7,-2] ns**	$\frac{N_{SR}}{N_{NVS}}$
Events before ΔR_{pull} cut	45	30	1.50 ± 0.12
Events after ΔR_{pull} cut	15	8	1.88 ± 0.38

Table 9: Number of events before and after our $\Delta R_{\text{pull}} > 5$ cut in the signal ([2,7] ns) and wrong-vertex sideband ([-7,-2] ns) regions for the $W \to e\nu \to \gamma_{\text{fake}} + \not\!\!E_T$ sample with the $E_{\text{T}}^0 > 45$ GeV cut for both photons and `MET(0)`.

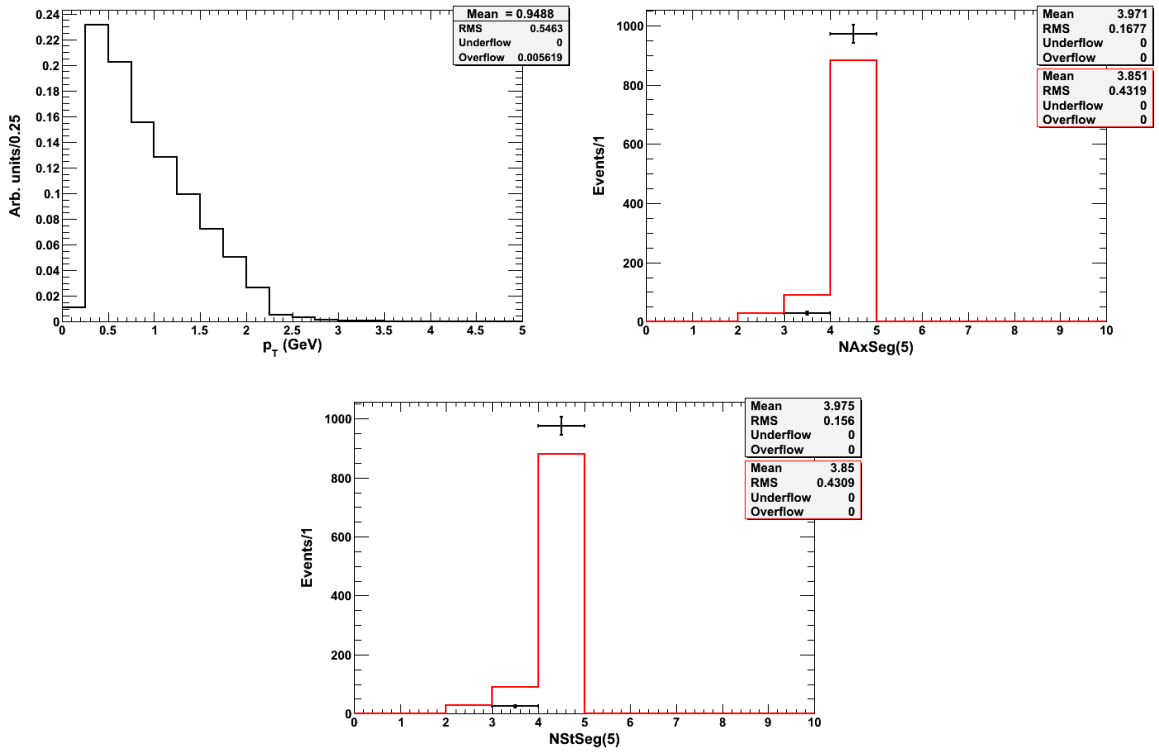

Figure 15: Left figure: The P_T distribution for tracks in the MC $W \to e\nu \to \gamma_{\text{fake}} + \not\!\!E_T$ sample that are rejected by our algorithm. Note that, as expected, most are low-P_T which is consistent with being from a hard-brem interaction with the detector. Number of axial (top right) and stereo (bottom) COT segments with five or more hits associated with closest *good* tracks in $e \to \gamma_{\text{fake}}$ events (black), compared to those associated with good electrons in MC $W \to e\nu \to e + \not\!\!E_T$events (red). Note that while the number of events with smaller number of segments is larger for $e \to \gamma_{\text{fake}}$ events, the overwhelming majority of tracks used for rejection have 4 good segments.

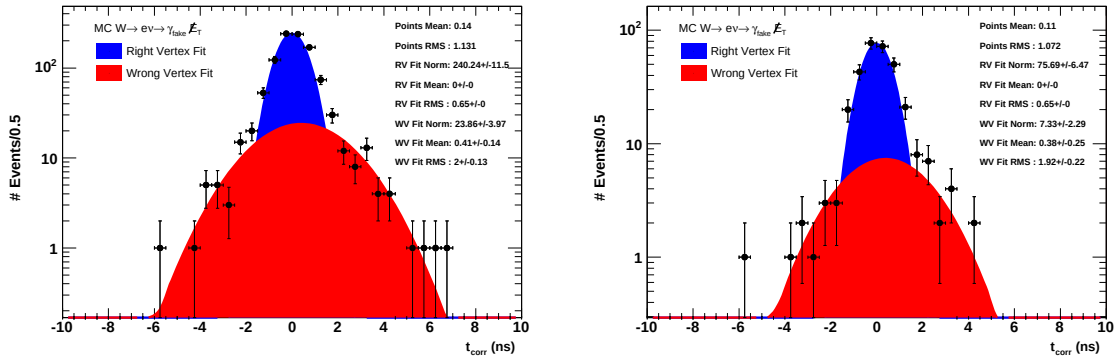

Figure 16: The timing distribution for photons candidate in the $W \to e\nu \to \gamma_{\rm fake} + \not\!\!E_T$ sample before (left) and after (right) the $\Delta R_{\rm pull} > 5$ cut are shown. The wrong vertex distribution parameters are allowed to float in the fit, illustrating that it doesn't change much even though the overall normalization does.

5 Cross-Checks of the Method

Before concluding, we report on a series of cross-checks of our method. One of our primary concerns is whether the rejection power and efficiency are the same in data and in Monte Carlo. While we can create a fairly pure sample of $e \to \gamma_{\rm fake}$ in data by trying to select $Z \to ee \to e\gamma_{\rm fake}$ events, this has the disadvantage that this sample is biased toward events where we are able to reconstruct one of the electrons. Similarly, it is non-trivial to determine the purity. For this reason, we only use this as a check rather than the primary method. A second set of independent checks is to address the concern as to whether the efficiency is insensitive to the number of tracks in the event. For example, if there are lots of tracks in an event the inefficiency due to a random track causing a good photon to be rejected can be significant and should rise as a function of the number of tracks in the event. We will show that this is not a problem for exclusive $\gamma + \not\!\!E_T$ samples by looking at the photon selection efficiency *vs.* the number of tracks in MC $Z\gamma \to \nu\nu\gamma \to \gamma + \not\!\!E_T$ events. We confirm this by considering the inefficiency of our cuts on a sample of $\gamma + \not\!\!E_T$ events from cosmics as the photon candidates will not be correlated with any of the tracks in the primary collision; this is one of the few sources of pure "photons" in real data. For the last cross-check we will relax the good track requirement used throughout this study, which would allow including SVX-only tracks to verify whether or not selecting only good COT tracks adversely affects the rejection power of our method. This will test whether or not the inclusion of silicon-only tracks, like those used in Phoenix tracking, would significantly improve our rejection.

5.1 Check of the Rejection Power Using $e \to \gamma_{\rm fake}$ in $Z \to ee \to e\gamma$ Events from Data and Monte Carlo

We start the series of cross-checks of our method by comparing our results to data to the best of our ability. We consider three samples: MC $W \to e\nu \to \gamma_{\rm fake} + \not\!\!E_T$, MC $Z \to ee \to e\gamma$ and data $e\gamma$. We will consider the rejection for these three samples as well as the shapes of the $\Delta\eta$ and $\Delta\phi$ distributions to see how well they agree. As we will see, both MC's are very consistent, but it's harder to tell in the data because of the purity. In particular, we are unable to properly measure the rejection factor, however the $\Delta\eta$ and $\Delta\phi$ distributions are very consistent.

The event selection for both the data and MC $e\gamma$ events to select the $Z \to ee \to e\gamma_{\rm fake}$ sample is shown in Table 6. We require a good electron and a good photon, and to improve the purity of events where the electron and photon candidate are associated with the decay of the Z boson, we require that the invariant mass of both objects be within $81 < M_{e\gamma} < 101$ GeV mass window. The invariant mass of the $e\gamma_{\rm fake}$ system before this cut is shown in Fig. 17. The invariant mass distribution outside this mass window shows that there is significant contribution from events that are not $Z \to ee \to e\gamma_{\rm fake}$. The contamination can come from different sources, such as $Z\gamma \to ee\gamma \to e_{\rm lost}e\gamma$ and $W\gamma \to e\nu\gamma$ in the low $\not\!\!E_T$ tail, etc. Figure 18 shows

the rejection factor as a function of mass. Unfortunately, the contamination makes it difficult to compute a proper rejection factor. We do observe a significant rise in rejection as we move into the peak region where the purity of $e \to \gamma_{\rm fake}$ should rise. We also note that outside the peak region the rejection rate does not decrease to the pure photon rejection rate due to real $e \to \gamma_{\rm fake}$ candidates contributing to $e\gamma$ events.

While a proper estimate requires a full understanding of the real $e\gamma$ and $e\gamma_{\rm fake}$ both inside and outside the Z mass window, we can compare the shapes of the $\Delta\eta$ and $\Delta\phi$ distributions. As can be seen in the top two plots in Fig. 19 (summarized in Table 10), both samples show a remarkable agreement, which results in the agreement in the $\Delta R_{\rm pull}$ distributions (top Fig. 20). While the agreement between the two different MC sources of $\gamma_{\rm fake}$ are nearly identical, the $\Delta\eta$ and $\Delta\phi$ agreement is fairly close visually, but is not as close for the $e\gamma$ sample from data (Fig 19, bottom) where we have required events to be within the invariant mass window. Also, as can be seen in Fig. 20 (bottom) we should not expect a good agreement between the MC samples and real data after applying the $\Delta R_{\rm pull}$ cut.

Samples

	MC $W \to e\nu \to \gamma_{\rm fake} + \not\!\!E_T$	MC $Z \to ee \to e\gamma_{\rm fake}$	$e\gamma$ (data)
$\sigma_{\mathbf{\Delta}\eta}$	0.0058 ± 0.0002	0.0058 ± 0.0002	0.0061 ± 0.0002
$\sigma_{\mathbf{\Delta}\phi}$	0.070 ± 0.003	0.066 ± 0.003	0.057 ± 0.003

Table 10: A comparison of the widths of $\Delta\eta$ and $\Delta\phi$ values for the MC $W \to e\nu \to \gamma_{\rm fake} + \not\!\!E_T$, MC $Z \to ee \to e\gamma_{\rm fake}$ and $e\gamma$ data samples (with Z selection) as measured from Fig. 19. All the values of $W \to e\nu \to \gamma_{\rm fake} + \not\!\!E_T$ and $Z \to ee \to e\gamma_{\rm fake}$ sets are in close agreement. The $e\gamma$ data shows a significant discrepancy from the other two sets which is likely due to purity issues discussed in the text. The errors quoted are statistical only.

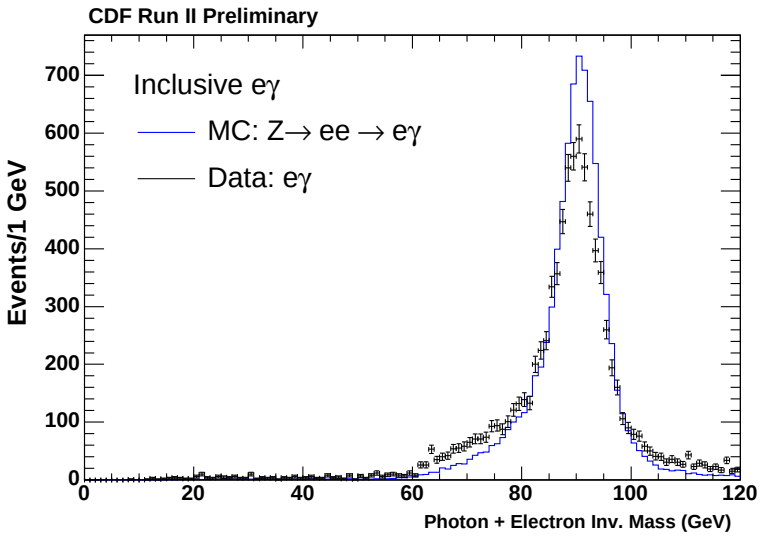

Figure 17: The invariant mass distribution of the $e\gamma$ data (crosses) and MC $Z \to ee \to e\gamma$ (solid line) with standard photon and electron identification (see Tables 2 and 3). The MC $Z \to ee \to e\gamma$ is normalized to the data.

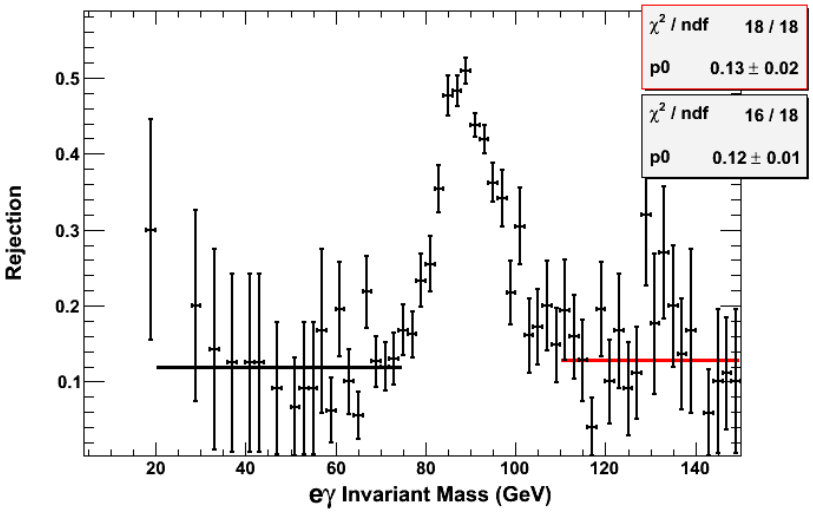

Figure 18: Rejection rate vs. invariant mass for the $e\gamma$ data sample. The mean rejection rates in the the $20 < M_{e\gamma} < 75$ GeV and $110 < M_{e\gamma} < 150$ GeV mass windows are approximately consistent.

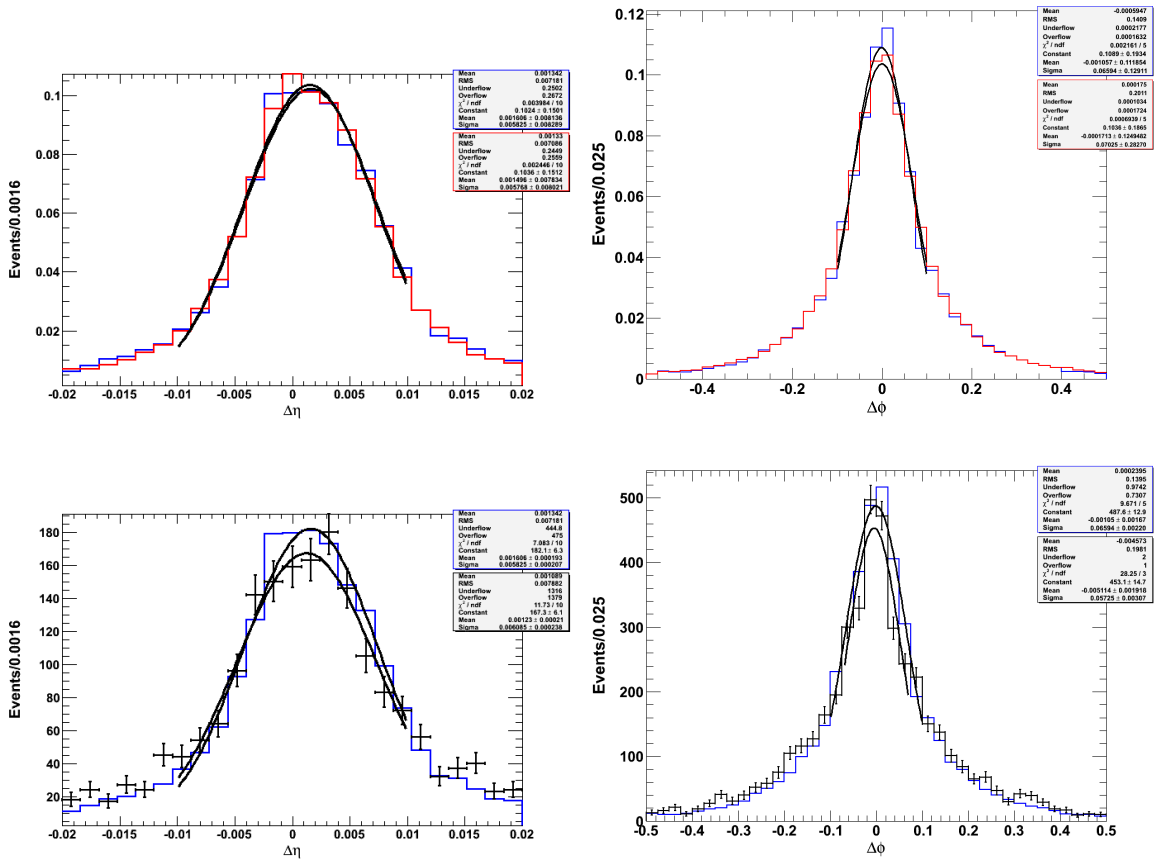

Figure 19: Top figures: the $\Delta\eta$ and $\Delta\phi$ distributions for MC $W \to e\nu \to \gamma_{\text{fake}} + \not{E}_T$ (red) and MC $Z \to ee \to e\gamma_{\text{fake}}$(blue) events. The widths of the peaks are in agreement. Bottom figures: The $\Delta\eta$ and $\Delta\phi$ distributions for $e\gamma$ data (black) in the Z mass window and MC $Z \to ee \to e\gamma_{\text{fake}}$(blue), with the latter normalized to $e\gamma_{\text{fake}}$ data. The data peaks are slightly wider than the MC due to the purity issues discussed in Section 5.1.

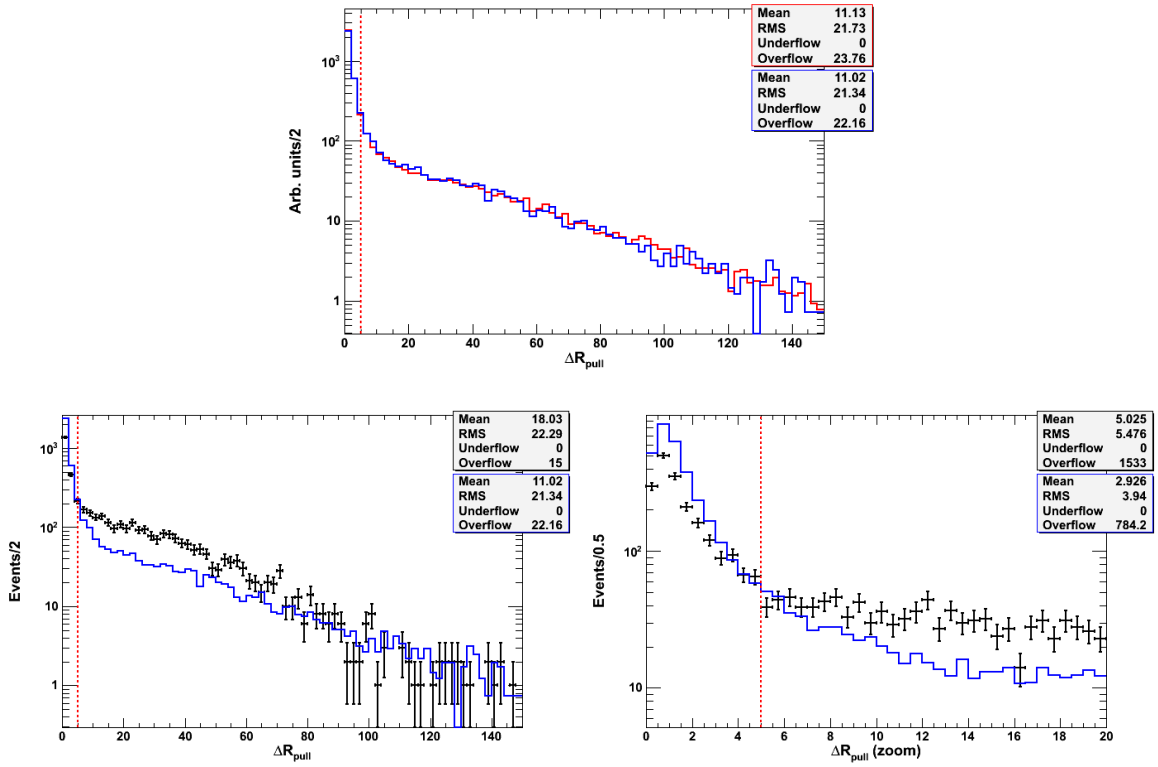

Figure 20: The ΔR_{pull} distribution for the MC $W \to e\nu \to \gamma_{\text{fake}} + \not{E}_T$ (red), $e\gamma$ data (black) and MC $Z \to ee \to e\gamma_{\text{fake}}$ (blue) events. The two MC samples agree nicely (top), but the data and MC distributions do not agree due to the purity issues discussed in Section 5.1. The ΔR_{pull} distribution for the $e\gamma$ data with $81 < m_{e\gamma} < 101$ GeV (black), $Z \to ee \to e\gamma_{\text{fake}}$ Monte Carlo (blue). The dashed lines show our chosen $\Delta R_{\text{pull}} > 5$ cut.

5.2 Efficiency Cross-Checks

Next we compare the efficiency of our cuts between data and MC, as well as a function of the number of tracks in the event. In principle, the presence of a large number of random extra tracks ought to reduce the efficiency of our cut since the probability of a track randomly pointing in the direction of the photon goes up. We next consider whether this is true for the typical numbers of tracks in our events. To study this we consider two samples: MC $Z\gamma \to \nu\nu\gamma \to \gamma + \not\!\!E_T$ events and a sample of photon candidates in cosmics events taken from real data (see Table 7). Since there is no good sample of pure photons in data, we select photon candidate events from cosmics since they are not likely to be from jets or electrons which would introduce an inefficiency bias due to the production of tracks in association with the calorimeter cluster. Note that these events are selected using the same requirements as the $\gamma + \not\!\!E_T$ events passing all the cuts in Table 3 where we have added the a timing window requirement of $20 < t_{\rm raw} < 80$ ns, well separated from the [-5, 5] ns interval, where the bulk of the $p\bar{p}$ collisions occur (see, e.g, Fig. 12 in Ref. [33]).

The efficiency of the $\Delta R_{\rm pull}$ cut as a function of the total number of tracks in the event is shown in Figs. 21 and 22. The overall average is $\sim 95\%$, but decreases slightly in a linear fashion over the number of tracks. Generally speaking, the probability of any random track falling within the $\Delta R_{\rm pull}$ cut is very low. This is not surprising as the photon candidates are already selected (see Table 2) by virtue of track isolation and an N3D track cut. However, as the total number of tracks increases, the efficiency drops because of the greater probability that a random track will fall within the $\Delta R_{\rm pull}$ cut. This implies that our method is robust and may be used for other types of analyses involving the standard tight photon selection. In Fig. 22, we show the $\Delta R_{\rm pull}$ distribution for the cosmics events superimposed on the MC $Z\gamma \to \nu\nu\gamma \to \gamma + \not\!\!E_T$ events. We note that the cosmics sample is distributed more heavily at lower $\Delta R_{\rm pull}$ values than the MC $Z\gamma \to \nu\nu\gamma \to \gamma + \not\!\!E_T$ events. This is explained by the NTrack distribution in the same figure which indicates that the cosmics sample also has a relatively stronger distribution at the higher NTrack values–an example of how events with many tracks will randomly have one in close proximity to the photon, yielding a relatively low $\Delta R_{\rm pull}$ value. The overall efficiency of the $\Delta R_{\rm pull}$ cut in the cosmics ($Z\gamma \to \nu\nu\gamma \to \gamma + \not\!\!E_T$) sample is 89% (92%) in exclusive samples (see Table 2).

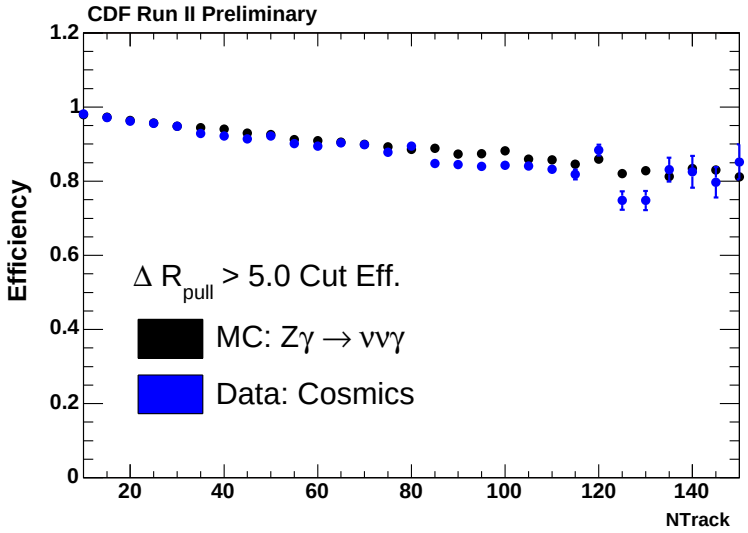

Figure 21: The efficiency of the $\Delta R_{\rm pull}$ cut on the MC $Z\gamma \to \nu\nu\gamma \to \gamma + \not\!\!E_T$ as a function of track multiplicity.

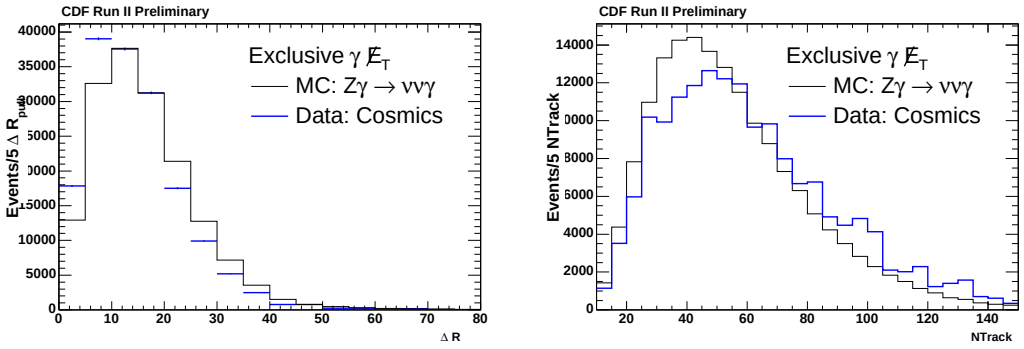

Figure 22: The $\Delta R_{\rm pull}$ distribution (left) and number of tracks (right) for the cosmics events, shown superimposed on the MC $Z\gamma \to \nu\nu\gamma \to \gamma + \not\!\!E_T$ events, where these are exclusive samples required to pass the selection requirements in Table 2. The NTracks distribution of the cosmics differs slightly from that of MC $Z\gamma \to \nu\nu\gamma \to \gamma + \not\!\!E_T$ events. This will cause the $\Delta R_{\rm pull}$ distribution to differ as well because as the number of tracks in a cosmic event–which are randomly distributed–increases, the relative distance between the photon and the closest track decreases.

5.3 Check of the Rejection Power with Looser Track Quality Requirements and Standalone SVX Tracks

We next check the robustness of our good track assumption (i.e., requiring `NAxSeg(5)` ≥ 2 and `NStSeg(5)` ≥ 2) and ask whether making a much looser selection on other tracks, like allowing standalone SVX tracks, would significantly improve our rejection power, without reducing the efficiency. To test this idea we eliminated the axial and stereo COT segment cuts and considered any track in the STNtuple to be the track closest to the photon in $\Delta R_{\rm pull}$, regardless of its quality. This looser selection also includes SVX-only tracks. We observe that we add, on average, about 20% more tracks. We find that the rejection increases by about 1% (as measured in our MC $W \to e\nu \to \gamma_{\rm fake} + \not\!\!E_T$ sample), while the efficiency decreases by about 1% (as measured in $Z\gamma \to \nu\nu\gamma \to \gamma + \not\!\!E_T$ sample). Thus, a looser selection, such as this one, does not add much rejection power, while at the same time it lessens the efficiency of the cut, since any poorly measured track can cause a real photon candidate to be rejected. We thus choose to keep the good track requirement in place, mostly for robustness reasons.

6 Summary

We have developed a new method to reject $e \to \gamma_{\text{fake}}$ candidates that pass the standard tight photon identification requirements. This is particularly useful for events where the primary vertex is not reconstructed, making the standard photon ID less powerful and makes the Phoenix tracking unhelpful. We need these additional handles especially in searches for new physics in $\gamma + \not\!\!E_T$ events. The new method matches tracks and photon candidates using beam-line properties of the tracks and takes into account the track reconstruction angular resolution for hard-brem electrons. Our method rejects $e \to \gamma_{\text{fake}}$ candidates $\approx 73\%$ of the time while keeping real photons $\approx 90\%$ of the time. This is consistent with the rejection and efficiency of the Phoenix method when the vertex that produced the electron is reconstructed as the primary vertex, but has the advantage that it works even if the vertex that produced the electron isn't reconstructed.

A Appendix: Timing for Photons from $e \to \gamma_{\mathbf{fake}}$

One of the dominant Standard Model backgrounds to the search for exclusive $\gamma_{\rm delayed} + \not\!\!E_T$, regardless of the production source of the photon candidate, is the choice of an incorrect vertex. The problem of wrong vertex selection has been discussed in detail in Ref. [13]. In this appendix we provide more detail on the motivation for removing events which might pick the wrong vertex, in particular it has a significant impact on the timing distribution. For this reason we describe the timing measurement and then continue with two of the biases that come from $W \to e\nu \to e + \not\!\!E_T$ events. To understand why these problems occur we start with the variable definitions used in delayed photon searches. These variables have been well described elsewhere [14]. This variable provides good separation power between prompt and delayed photon.

The variable $t_{\rm corr}$ is defined to be the difference between the measured time of arrival recorded by the calorimeter EMTiming systems [17] and the collision time, recorded using the COT and vertexing algorithms, and the expected times of flight of the photon between the assumed primary vertex [13] as measured from the position in the CES and vertex respectively. We take

$$t_{\rm corr} \equiv (t_f - t_i) - \frac{|\vec{x_f} - \vec{x_i}|}{c}, \tag{9}$$

where $t_f - t_i$ is the *true* time of flight between the arrival point in the calorimeter and the collision point, respectively, and $\frac{|\vec{x}_f - \vec{x}_i|}{c}$ is the *measured* distance $|\vec{x_f} - \vec{x_i}|$ between the arrival point and the assumed vertex position, respectively, divided by the speed of light, c. With this definition, assuming perfect measurements and the selection of the correct vertex, a prompt photon would have $t_{\rm corr} = 0$; a long-lived $\tilde{\chi}_1^0$ that decays to a photon, as shown in Fig. 3, would have a measured $t_{\rm corr} \geq 0$. In other words, it would arrive delayed relative to expectations. True measurement uncertainties smear the $t_{\rm corr}$ of promptly produced photons to be a Gaussian centered at zero with a width of 0.65 ns. The selection of the wrong vertex (yielding uncorrelated values of $\vec{x_i}$ and t_i) is problematic and has a width of 2.05 ns for most scenarios [17]. The mean of the distribution is typically zero, but can be biased for various reasons [16]. The typical search for delayed photons selects events with $t_{\rm corr} \geq$ 2 ns, which cuts away from the majority of the SM background events with a correctly selected vertex, regardless of their source. Thus, the dominant background source is events with a wrong vertex (and cosmics). The amount of wrong vertex event can be estimated from the number of events with $t_{\rm corr} \leq -2$ ns, if the mean of the timing distribution is well measured and/or understood [34].

A.1 Promotion Effect in $W \to e\nu \to \gamma_{\mathbf{fake}} + \not\!\!E_T$ Events

It turns out that $W \to e\nu \to \gamma_{\rm fake} + \not\!\!E_T$ events often have the wrong vertex selected and do so in ways that further exacerbate problems in searches for GMSB in exclusive $\gamma_{\rm delayed} + \not\!\!E_T$ events. Specifically, the ways that electrons fake photons, and the E_T

distribution of electrons from $W \to e\nu \to \gamma_{\rm fake} + \not\!\!E_T$ events can both bias the mean of the wrong-vertex timing distribution as well as significantly change the content of the sample. We explain this next, following the discussion in Ref. [16], but note for now that equally important is that in addition to affecting the $t_{\rm corr}$in Eq.9, the selection of the wrong vertex affects the photon's E_T measurement. The measurement of E_T and the timing for photon candidates are correlated for wrong vertex events. For photons we define E_T as $E_T \equiv E \sin\theta$, where E is measured from the calorimeter, and θ is measured using the CES position in the calorimeter and the presumed vertex position in z. Consider, for example, the configuration in Fig. 23 where the vertexing algorithm does not select the correct collision point either because it is not reconstructed or because a higher ΣP_Tvertex from min-bias exists. In this case we have $\theta_{\rm measured} > \theta_{\rm true}$, so that $|\vec{x_f} - \vec{x}_{\rm measured}| < |\vec{x_f} - \vec{x}_{\rm true}|$, resulting in $t_{\rm corr}^{\rm measured} > t_{\rm corr}^{\rm true}$ in Eq. 9 (ignoring the contribution from t_i). At the same time, since $\theta_{\rm measured} > \theta_{\rm true}$, we find $E_T^{\rm measured} > E_T^{\rm true}$. The converse is also true: a configuration with a mismeasured vertex, where $\theta_{\rm measured} < \theta_{\rm true}$, would lead to a lower measured value of $t_{\rm corr}$ and lower measured value of E_T. To summarize: when $E_T^{\rm measured} > E_T^{\rm true}$, $t_{\rm corr}^{\rm measured} > t_{\rm corr}^{\rm true}$; conversely, for $t_{\rm corr}^{\rm measured} > t_{\rm corr}^{\rm true}$, $E_T^{\rm measured} > E_T^{\rm true}$. Thus, misidentification of vertices leads to values of $t_{\rm corr}$ and E_T being shifted in the same direction.

The migration of E_T values due to the incorrect vertex selection can also significantly affect the composition of the events in the sample. This is readily seen because a typical analysis requires $E_T^{\rm measured} > E_T^{\rm cut}$. Thus, events that have $E_T^{\rm true} < E_T^{\rm cut} < E_T^{\rm measured}$ will enter the sample, as well as have $t_{\rm corr}^{\rm measured} > t_{\rm corr}^{\rm true}$. In other words, events that just make it into the sample will be biased toward larger times. At the same time, the events with $E_T^{\rm true} > E_T^{\rm cut} > E_T^{\rm measured}$ will leave the sample and for these events $t_{\rm corr}^{\rm measured} < t_{\rm corr}^{\rm true}$, a second bias towards smaller times. In other words, events that migrate into the sample have large times and events that leave the sample have smaller times. While this might not be a big effect in principle, the number of events entering and leaving around an E_T cut is frequently asymmetric. A striking example of this is seen in an MC sample of $W \to e\nu \to \gamma_{\rm fake} + \not\!\!E_T$ events with a cut of $E_T^{\rm measured} > 45$ GeV, as seen in Fig. 24. Since there are more events with small $E_T^{\rm true}$ than large $E_T^{\rm true}$, more events events make it past the value of $E_T^{\rm cut}$, resulting in a higher average value of $t_{\rm corr}$ when the wrong vertex is selected. At 45 GeV the slope of the $E_T^{\rm true}$ distribution is very sharp around the cut boundary, so the migration effect is very significant.

A.2 Path Length Effects for Electrons

The second effect that impacts the mean of the wrong-vertex timing for $W \to e\nu \to \gamma_{\rm fake} + \not\!\!E_T$ events is that an electron is more likely to fake a photon if its path length from its collision point to the calorimeter face is longer. A longer path length means that $|\vec{x}_f - \vec{x}_{\rm measured}| < |\vec{x}_f - \vec{x}_{\rm true}|$, producing a bias towards $E_T^{\rm measured} > E_T^{\rm true}$, and thus $t^{\rm measured} > t^{\rm corr}$, so the same bias arguments hold. When both effects are combined, the mean timing shift can be of the order of 800 ps (see Fig. 24), which can more than double the number of events in the signal timing window (2 ns $< t_{\rm corr} <$ 7 ns), relative

to the no-vertex sideband region at negative times (-7 ns $< t_{\rm corr} <$ -2 ns).

The bottom line is that $W \to e\nu \to \gamma_{\rm fake} + \not\!\!E_T$ backgrounds are significant in all searches with final state photons and $\not\!\!E_T$ but particularly problematic in events where we consider the timing of the photon and have problems picking the correct vertex. All these problems are present in the search for GMSB with Higgs production in the exclusive $\gamma_{\rm delayed} + \not\!\!E_T$ final state.

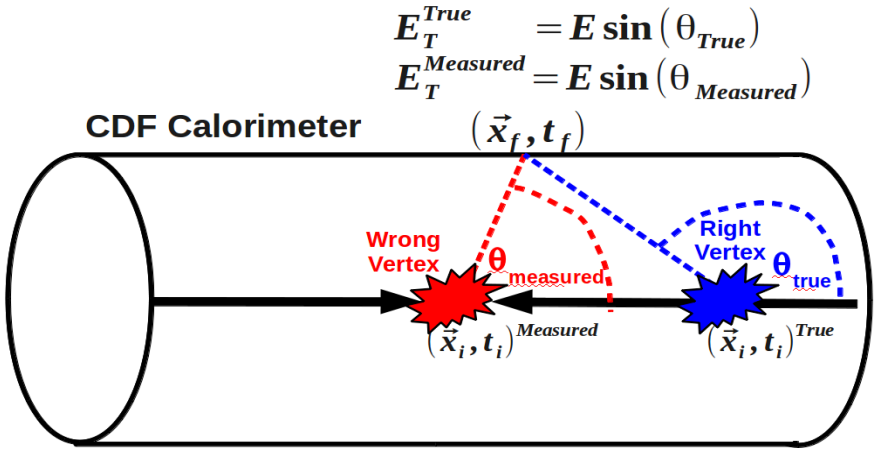

Figure 23: A cartoon drawing of a $W \to e\nu \to \gamma_{\rm fake} + \not\!\!E_T$ event with a misidentified vertex. In this case, the wrong vertex selection leads to an angle $\theta_{\rm measured}$ larger than the real angle $\theta_{\rm true}$, which results in a larger measured value of $E_T (E_T^{\rm measured} > E_T^{\rm true})$. If the wrong vertex is selected, then the apparent path is shorter than the true path, leading to the incorrect conclusion that the photon took longer to arrive than a direct path would imply [16].

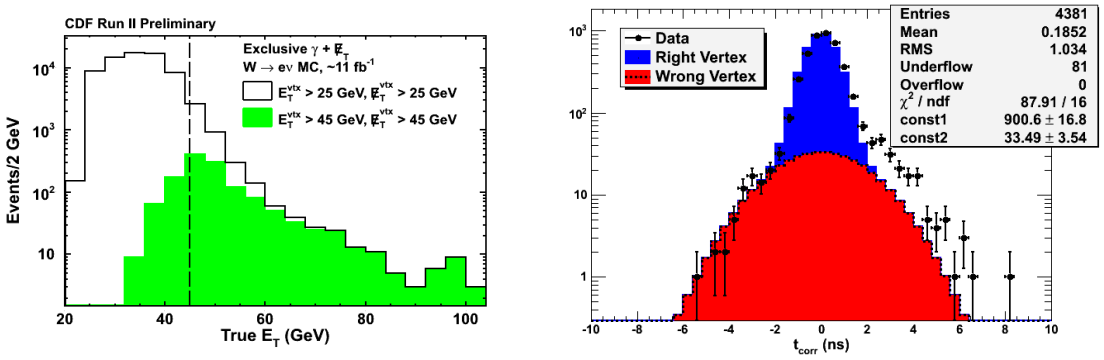

Figure 24: Left: Promotion and demotion of E_T values around the $E_T > 45$ GeV cut for an MC sample of $W \to e\nu \to \gamma_{\text{fake}} + \not\!\!E_T$ events. The unshaded histogram is the true E_T for electrons that fake photons, the solid histogram (shown in green) is the true E_T for electrons that were identified as photons, and passed the $E_T^{\text{measured}} > 45$ GeV cut. The plot shows more events entering the sample than leaving it. Right: The t_{corr} distribution for the sample of simulated $W \to e\nu \to \gamma_{\text{fake}} + \not\!\!E_T$ events that pass the $E_T^{\text{measured}} > 45$ Gev cut. (More details on how this sample is created in Section 3, Table 4). The two Gaussian distributions are calculated with the old, naïve assumption that their mean is centered around $t_{\text{corr}} = 0$ ns [17] but normalized between -7 ns and 2 ns. Note the "expected" excess for times between 2 and 7 ns. For the sample, the average time of the wrong-vertex events are shifted to higher times for the reasons given in the text. This can be misidentified as a signal for long-lived $\tilde{\chi}_1^0$.

B Appendix: On the Possibility Using the $q\Delta\phi$ Method to Reject Fakes

As noted in Section 4.1, the direction of $\Delta\phi$, as defined in Eq. 2, is correlated with the charge of the electron. Thus, it is natural to think that taking into account the charge of the track can provide additional rejection power. If the track is well reconstructed, the product of $\Delta\phi$ and the charge associated with the track will be always greater than zero due to the direction of the magnetic field. As can be seen in Fig. 25, top left, which shows electrons selected using the $W \to e\nu \to e + \not{E}_T$ sample, selected using the requirements in Table 8, this is indeed the case for good electrons and positrons.

We attempted to see whether making a $q\Delta\phi$-related cut might help improve the rejection without sacrificing the efficiency. To this end, we used the MC $W \to e\nu \to \gamma_{\rm fake} + \not{E}_T$ and $Z\gamma \to \nu\nu\gamma \to \gamma + \not{E}_T$ control samples. In the top right figure we show $q\Delta\phi/0.081$ distributions (0.081 being the same value used in defining the $\Delta R_{\rm pull}< 5$ cut), but without any cut on $\Delta\eta$. While the peak is sharp, there are tails to negative times even for $e \to \gamma_{\rm fake}$ events. However, these are from events where the right track isn't reconstructed at all so it might be that they can be ignored. To check this we require $|\Delta\eta| < 0.006$. Next we examined two other potential selections: the $q\Delta\phi$ distribution after applying the $\Delta\eta = 0.006$ cut and $(q\Delta\phi)p_T$ (second and third row of Fig. 25, respectively). The left and right sides of the middle row show the results before and after the $\Delta\eta < 0.006$ cut, the same value used in defining the $\Delta R_{\rm pull}< 5$ cut. We see that the tail is cleaned up, but that the RMS of the distribution isn't significantly helped compared to the regular $\Delta\phi$ distribution. However, the width of the $q\Delta\phi$ distribution is less important than the tails, we can get back some efficiency only by requiring $q\Delta\phi > 0$. By tightening the cut to get the same efficiency for a better rejection doesnt help much since there isnt much background here. Thus, since it does not offer any additional rejection power as compared to our chosen $\Delta R_{\rm pull}$ cut, the combination of $\Delta\eta$ and $q\Delta\phi$ cuts was not chosen as our preferred cut. We note that for events with large number of tracks, where the inefficiency might get large, this might be a useful additional cut.

One final idea was to consider the $(q\Delta\phi)p_T$ distributions as they should be a constant for a constant magnetic field in an attempt to achieve better $W \to e\nu \to \gamma_{\rm fake}+\not{E}_T$ and $Z\gamma \to \nu\nu\gamma \to \gamma+\not{E}_T$ separation. The idea that the track from a fake photon might be significantly lower in P_T than a random track for the $Z\gamma \to \nu\nu\gamma \to \gamma+\not{E}_T$ sample. It can be clearly seen that $q\Delta\phi$ is a better distribution to make a cut on than $(q\Delta\phi)p_T$ because the p_T is not well measured for the track (being due to a Brem) since the $Z\gamma \to \nu\nu\gamma \to \gamma + \not{E}_T$ background is broader in the former case, affecting the efficiency less.

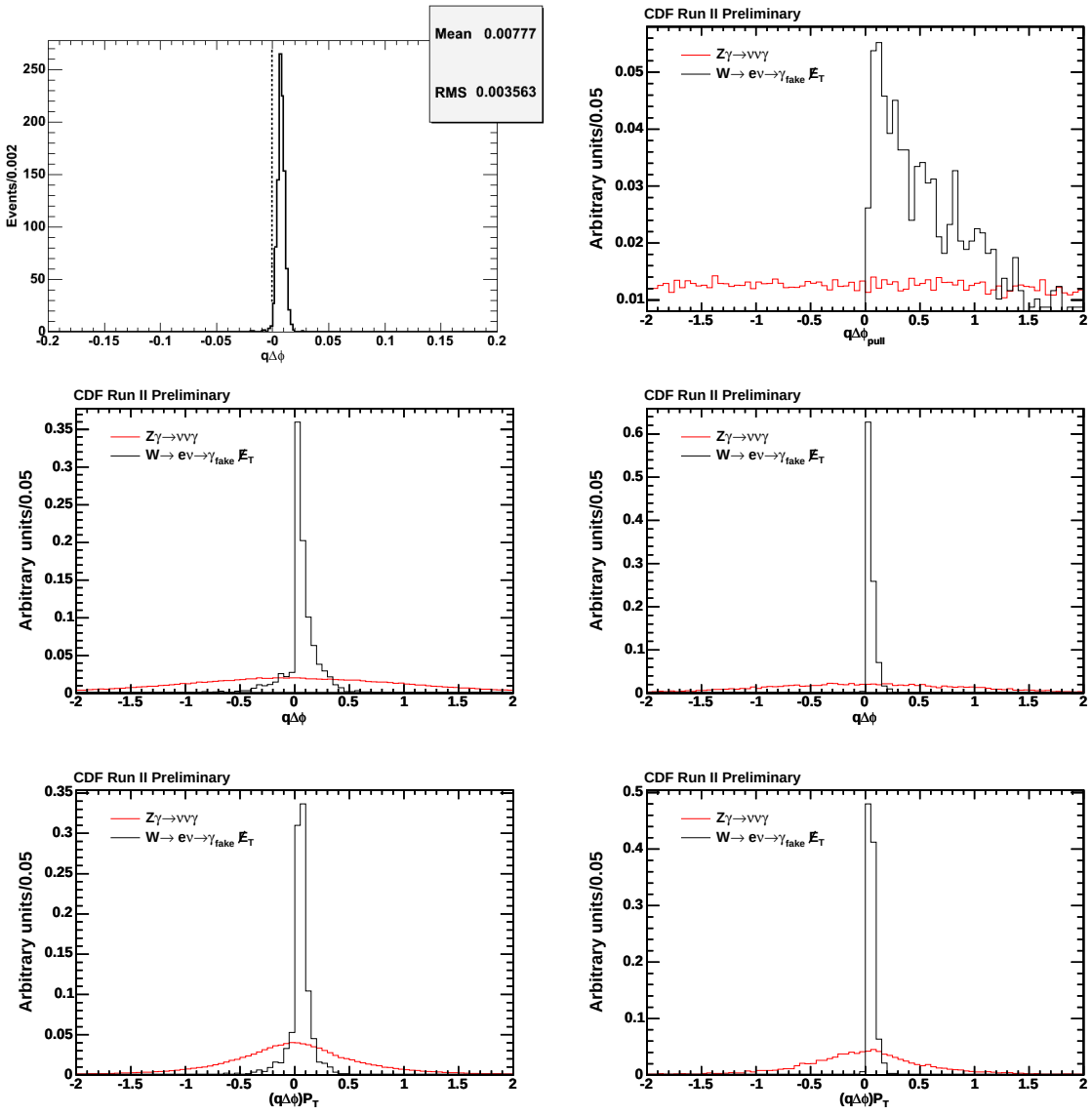

Figure 25: The distributions involving $q\Delta\phi$ variable (see text for more details). Top left: The $q\Delta\phi$ distribution for good electrons. Top right: The $q\Delta\phi/0.081$ distributions for the MC $W \to e\nu \to \gamma_{\rm fake} + \not\!\!E_T$ (black) and $Z\gamma \to \nu\nu\gamma \to \gamma + \not\!\!E_T$ samples (red). Middle: The $q\Delta\phi$ distributions before (left) and after (right) the $|\Delta\eta| < 0.006$ cut for the MC $W \to e\nu \to \gamma_{\rm fake} + \not\!\!E_T$ and $Z\gamma \to \nu\nu\gamma \to \gamma + \not\!\!E_T$. Bottom: $(q\Delta\phi)p_T$ before (left) and after (right) the $|\Delta\eta| < 0.006$ cut for the MC $W \to e\nu \to \gamma_{\rm fake} + \not\!\!E_T$ and $Z\gamma \to \nu\nu\gamma \to \gamma + \not\!\!E_T$.

References

[1] Tight Photon Selection (`http://www-cdf.fnal.gov/htbin/twiki/bin/view/Main/TightPhotonSelection`). 3, 8, 10, 14

[2] T. Nelson, R. Snider, D. Stuart, "Forward Electron Tracking with the PhoenixMods Package," CDF Note 6278 (2003). 3, 8, 9, 25

[3] P. Fayet, "Mixing Between Gravitational and Weak Interactions Through the Massive Gravitino," *Phys. Lett.* **B 70** (1977) 461. M. Dine, A. E. Nelson, Y. Nir and Y. Shirman, "New tools for low-energy dynamical supersymmetry breaking," *Phys. Rev.* **D 53** (1996) 2658, [arXiv:hep-ph/9507378]; H. Baer, M. Brhlik, C. h. Chen and X. Tata, "Signals for the minimal gauge mediated supersymmetry breaking model at the Fermilab Tevatron collider," *Phys. Rev.* **D 55** (1997) 4463, [arXiv:hep-ph/9610358]. H. Baer, P. G. Mercadante, X. Tata and Y. l. Wang, "The Reach of Tevatron upgrades in gauge mediated supersymmetry breaking models," *Phys. Rev.* **D 60** (1999) 055001, [arXiv:hep-ph/9903333]; S. Dimopoulos, S. D. Thomas and J. D. Wells, "Sparticle spectroscopy and electroweak symmetry breaking with gauge mediated supersymmetry breaking," *Nucl. Phys.* **B 488** (1997) 39, [arXiv:hep-ph/9609434]; J. R. Ellis, J. L. Lopez and D. V. Nanopoulos, "Analysis of LEP constraints on supersymmetric models with a light gravitino," *Phys. Lett.* **B 394** (1997) 354, [arXiv:hep-ph/9610470]. 4, 6

[4] T. Appelquist, H. C. Cheng and B. A. Dobrescu, "Bounds on Universal Extra Dimensions," *Phys. Rev.* **D 64** (2001) 035002, [arXiv:hep-ph/0012100v2]; H. -C. Cheng, J. L. Feng, K. T. Matchev, "Kaluza-Klein dark matter," *Phys. Rev. Lett.* **89** (2002) 211301, [arXiv:hep-ph/0207125v2]; G. Servant and T. M. P. Tait, "Is the lightest Kaluza-Klein particle a viable dark matter candidate?," *Nucl. Phys.* **B 650** (2003) 391, [arXiv:hep-ph/0206071]. 4

[5] G. R. Farrar and P. Fayet, "Bounds On R Hadron Production From Calorimetry Experiments," *Phys. Lett.* **B 79** (1978) 442, [arXiv:hep-ph/0408248v1]. 4

[6] D. A. Toback and P. Wagner, "Prospects of searches for neutral, long-lived particles which decay to photons using timing at CDF," *Phys. Rev.* **D 70** (2004) 114032, [arXiv:hep-ph/0407022v1]; J. D. Mason and D. Toback, "Prospects of Searches for Gauge Mediated Supersymmetry with $h^0 \to \chi_1^0\chi_1^0$ production in the Time-Delayed Photon + MET Final State at the Tevatron," Phys. Lett. B **702**, 377 (2011) [arXiv:1105.2194 [hep-ph]]. 4, 5

[7] LEP SUSY Working Group, ALEPH, DELPHI, L3, and OPAL Collaborations, LEPSUSYWG/04-09.1 (`http://lepsusy.web.cern.ch`); A. Heister *et al.* [ALEPH Collaboration], "Search for gauge mediated SUSY breaking topologies in e^+e^- collisions at center-of-mass energies up to 209 GeV,"

Eur. Phys. J. **C 25** (2002) 339 [arXiv:hep-ex/0203024]; M. Gataullin, S. Rosier, L. Xia and H. Yang, "Searches for gauge-mediated SUSY breaking topologies with the L3 detector at LEP," AIP Conf. Proc. **903**, 217 (2007) [arXiv:hep-ex/0611010]; G. Pasztor, "Search for gauginos and gauge mediated SUSY breaking scenarios at LEP," PoS **HEP2005**, 346 (2006) [arXiv:hep-ex/0512054]; J. Abdallah *et al.* [DELPHI Collaboration], "Search for one large extra dimension with the DELPHI detector at LEP," *Eur. Phys. J.* **C 60** (2009) 17 [arXiv:0901.4486 [hep-ex]]. 4, 5

[8] B. Abbott *et al.* [D0 Collaboration], "Experimental search for chargino and neutralino production via gauge mediated supersymmetry breaking models," *Phys. Rev. Lett.* **80** (1998) 442, [arXiv:hep-ex/9708005]; F. Abe *et al.* [CDF Collaboration], "Searches for new physics in diphoton events in $p\bar{p}$ collisions at $\sqrt{s} = 1.8$ TeV," *Phys. Rev. Lett.* **81** (1998) 1791, [arXiv:hep-ex/9801019]; F. Abe *et al.* [CDF Collaboration], "Searches for new physics in diphoton events in $p\bar{p}$ collisions at $\sqrt{s} = 1.8$ TeV," *Phys. Rev.* **D 59** (1999) 092002, [arXiv:hep-ex/9806034]; V. M. Abazov *et al.* [D0 Collaboration], "Search for supersymmetry with gauge-mediated breaking in diphoton events at D0," *Phys. Rev. Lett.* **94** (2005) 041801, [arXiv:hep-ex/0408146]; T. Aaltonen *et al.* [CDF Collaboration], "Search for Supersymmetry with Gauge-Mediated Breaking in Diphoton Events with Missing Transverse Energy at CDF II," *Phys. Rev. Lett.* **104** (2010) 011801, [arXiv:0910.3606 [hep-ex]]; V. M. Abazov *et al.* [D0 Collaboration], "Search for dark photons from supersymmetric hidden valleys," *Phys. Rev. Lett.* **103** (2009) 081902, [arxiv:hep-ex/0905.1478v2]. 4, 5, 8, 47

[9] G. Aad *et al.* [ATLAS Collaboration], "Search for Diphoton Events with Large Missing Transverse Energy in 7 TeV Proton-Proton Collisions with the ATLAS Detector," arXiv:1012.4272 [hep-ex]; S. Chatrchyan *et al.* [CMS Collaboration], "Search for Supersymmetry in pp Collisions at $\sqrt{s} = 7$ TeV in Events with Two Photons and Missing Transverse Energy," [arXiv:hep-ex/1103.0953] submitted to Phys. Rev. Lett.; 4, 5

[10] B. C. Allanach *et al.*, "The Snowmass points and slopes: Benchmarks for SUSY searches," in *Proc. of the APS/DPF/DPB Summer Study on the Future of Particle Physics (Snowmass 2001)* ed. N. Graf, *Eur. Phys. J.* **C 25** (2002) 113, [arXiv:hep-ph/0202233]. 4

[11] J. D. Mason, D. E. Morrissey and D. Poland, "Higgs Boson Decays to Neutralinos in Low-Scale Gauge Mediation," *Phys. Rev.* **D 80** (2009) 115015, [arXiv:0909.3523 [hep-ph]]. 4, 6

[12] See for example: H. Pagels and J. R. Primack, "Supersymmetry, Cosmology and New TeV Physics," *Phys. Rev. Lett.* **48** (1982) 223. 5

[13] T. Aaltonen *et al.* [CDF Collaboration], "Search for Heavy, Long-Lived Neutralinos that Decay to Photons at CDF II Using Photon Timing," *Phys. Rev.* **D 78** (2008) 032015, [arXiv:0804.1043 [hep-ex]]; A. Abulencia *et al.* [CDF Collaboration], "Search for heavy, long-lived particles that decay to photons at CDF II," *Phys. Rev. Lett.* **99** (2007) 121801, [arXiv:0704.0760 [hep-ex]]. 5, 39

[14] T. Aaltonen *et al.* [CDF Collaboration], "Search for large extra dimensions in final states containing one photon or jet and large missing transverse energy produced in $p\bar{p}$ collisions at $\sqrt{s}$ = 1.96-TeV," *Phys. Rev. Lett.* **101** (2008) 181602, [arXiv:0807.3132 [hep-ex]]. 5, 39

[15] D. E. Acosta *et al.* [CDF Collaboration], "Search for anomalous production of diphoton events with missing transverse energy at CDF and limits on gauge-mediated supersymmetry-breaking models," *Phys. Rev.* **D 71** (2005) 031104, [arXiv:hep-ex/0410053]. 7

[16] A. Aurisano, J. Asaadi, D. Goldin and D. Toback, "Study of the Timing of e to Fake Photon for Delayed Photon Analyses," CDF Note 9924. 39, 40, 41

[17] M. Goncharov *et al.*, "The Timing system for the CDF electromagnetic calorimeters," *Nucl. Instrum. Meth.* **A565** (2006) 543, [arXiv:physics/0512171]. 10, 16, 39, 42

[18] R. Culbertson, M. Goncharov, E. Lee, S. Pronko and D. Toback, "Setting Limits on GMSB Models in gg+Met Final State at CDF," CDF Note 9625 (2008). Published in Ref. [8]. 10, 14

[19] R.E. Kalman, "A new approach to linear filtering and prediction problems," J. Basic Eng. 82 (1960) 35; R.E. Kalman, R.S. Bucy, "New results in linear filtering and prediction theory," J. Basic Eng. 83 (1961) 95; M. Bedeschi, "Tracking, Vertexing and Alignment Basics," CDF Note 6743 (2003). 10

[20] A. Aurisano, J. Asaadi, D. Goldin and D. Toback, "The Search For New Physics in Exclusive Delay Photons + MET," CDF Note 10787. 12, 15

[21] R. Culbertson, A. Pronko, Shin-Shan Eiko Yu "The Probability of an Electron Faking an Isolated Prompt Photon in CEM." CDF Note 8220 (2009). 10

[22] T. Sjostrand, P. Eden, C. Friberg, L. Lonnblad, G. Miu, S. Mrenna and E. Norrbin, "High-energy-physics event generation with PYTHIA 6.1," *Comput. Phys. Commun.* **135** (2001) 238, [arXiv:hep-ph/0010017]. 12, 13

[23] CDFSim webpage: `http://www-cdf.fnal.gov/cdfsim/cdfsim_main.html` 12, 13, 17

[24] Official CDF Electroweak Group Monte Carlo Samples: (http://www-cdf.fnal.gov/physics/ewk/mc_samples.html). 12, 13

[25] Loose electron selection (http://www-cdf.fnal.gov/htbin/twiki/bin/view/Main/LooseElectronSelection). 14

[26] Vertex selection (http://www-cdf.fnal.gov/htbin/twiki/bin/view/Main/GoodVertexSelection). 15

[27] M.Goncharov, V.Krutelyov, D.Toback and P.Wagner, "Space-Time Vertex Reconstruction Using COT Tracks," CDF Note 8015 (2006). 15

[28] A. Aurisano, J. Asaadi, D. Goldin and D. Toback, "The Search For New Physics in Exclusive Delay Photons + MET," CDF Note 10787. 14

[29] Beam Halo selection (http://www-cdf.fnal.gov/htbin/twiki/bin/view/Main/BeamHaloRejectionCuts). 16

[30] TStnTrack class definition (http://www-cdf.fnal.gov/CdfCode/source/Stntuple/Stntuple/obj/TStnTrack.hh). 20

[31] Stntuple class definition (http://www-cdf.fnal.gov/CdfCode/source/Stntuple/). 20

[32] TStnPhoton class definition (http://www-cdf.fnal.gov/CdfCode/source/Stntuple/Stntuple/obj/TStnPhoton.hh). 20

[33] M. Goncharov, V.Krutelyov, A.Pronko, R.Culbertson, D.Toback, and P.Wagner, "Discrimination of Beam Halo and Cosmic Rays as a Source of Photon Candidates," CDF Note 8409 (2006). 35

[34] A. Aurisano, J. Asaadi, D. Goldin, J. Nett and D. Toback, "Background Estimation Methods in the Exclusive Delayed Photon + MET Final State" CDF Note 10790 (2012). 39